Pericytes support neutrophil subendothelial cell crawling and breaching of venular walls in vivo.

Proebstl, D; Voisin, M-B; Woodfin, A; Whiteford, J; D'Acquisto, F; Jones, GE; Rowe, D; Nourshargh, S

Pericytes support neutrophil subendothelial cell crawling and breaching of venular walls in vivo

Doris Proebstl,[1] Mathieu-Benoît Voisin,[1] Abigail Woodfin,[1] James Whiteford,[1] Fulvio D'Acquisto,[1] Gareth E. Jones,[2] David Rowe,[3] and Sussan Nourshargh[1]

[1]William Harvey Research Institute, Barts and The London School of Medicine and Dentistry, Queen Mary University of London, London EC1M 6BQ, UK
[2]Randall Division, King's College London, Guy's Campus, London SE1 1UL, UK
[3]Department of Genetics and Developmental Biology, University of Connecticut Health Center, Farmington, CT 06030

Neutrophil transmigration through venular walls that are composed of endothelial cells (ECs), pericytes, and the venular basement membrane is a key component of innate immunity. Through direct analysis of leukocyte–pericyte interactions in inflamed tissues using confocal intravital microscopy, we show how pericytes facilitate transmigration in vivo. After EC migration, neutrophils crawl along pericyte processes to gaps between adjacent pericytes in an ICAM-1–, Mac-1–, and LFA-1–dependent manner. These gaps were enlarged in inflamed tissues through pericyte shape change and were used as exit points by neutrophils in breaching the venular wall. The findings identify previously unknown roles for pericytes in neutrophil transmigration in vivo and add additional steps to the leukocyte adhesion cascade that supports leukocyte trafficking into sites of inflammation.

CORRESPONDENCE
Sussan Nourshargh:
s.nourshargh@qmul.ac.uk

Abbreviations used: 3D, three dimensional; 4D, four dimensional; αSMA, α smooth muscle actin; EC, endothelial cell; EGFP, enhanced GFP; ICAM-1, intercellular adhesion molecule-1; i.m., intramuscular; i.s., intrascrotal; IVM, intravital microscopy; MFI, mean fluorescence intensity; PECAM-1, platelet EC adhesion molecule-1; RFPcherry, red fluorescent protein cherry; TEM, tran-EC migration.

Transmigration of neutrophils from the vascular lumen through venular walls into the surrounding tissue is a vital response in host defense reactions during injury and infection and also a major cause of numerous inflammatory disorders. The venular wall is composed of two cellular components, endothelial cells (ECs) and pericytes, and a noncellular matrix protein structure called the vascular basement membrane (BM), which is generated by both ECs and pericytes (Nourshargh et al., 2010). In recent years, our understanding of the mode and molecular pathways mediating neutrophil migration through ECs has substantially enhanced (Ley et al., 2007; Muller, 2009). Although this response can occur relatively rapidly in vivo (~4–6 min; Woodfin et al., 2011), full breaching of the venular wall takes significantly longer (~15–40 min; Katori et al., 1990; Ley et al., 1993; Yadav et al., 2003), suggesting a considerable transit time through other components of the vessel wall. In this context, despite recent insights into leukocyte–BM interactions (Rowe and Weiss, 2008; Nourshargh et al., 2010), at present almost nothing is known about neutrophil–pericyte interactions in vivo and the potential role of pericytes in leukocyte transmigration. These key issues were the focus of the present investigation.

Pericytes are long cells (~70 µm in length) surrounding the EC layer of capillaries, postcapillary venules, and collecting venules, and are embedded within the venular BM (Shepro and Morel, 1993; Hirschi and D'Amore, 1996). Pericytes are closely associated with the endothelium, and play a critical role in maintaining the integrity of the vessel wall and contributing to the generation of the venular BM (Cohen et al., 1980; Mandarino et al., 1993; Armulik et al., 2005; Edelman et al., 2006). Pericytes exhibit morphological and phenotypic differences depending on vessel type, vascular bed, developmental stage, species, and pathological conditions (Hirschi and D'Amore, 1996; Sims, 2000), rendering their study in vivo and culture in vitro complex. As a result, the role of pericytes in inflammation and leukocyte trafficking

D. Proebstl and M.B. Voisin contributed equally to this paper.

The Rockefeller University Press $30.00
J. Exp. Med. Vol. 209 No. 6 1219-1234
www.jem.org/cgi/doi/10.1084/jem.20111622

remains largely unexplored. In most tissues, the pericyte network is discontinuous around the endothelium of postcapillary venules, with gaps between adjacent cells. The extent of pericyte coverage around microvessels varies substantially in different organs, suggesting different properties in different tissues.

Previous studies from our group have shown that neutrophils breach the pericyte layer by migrating through gaps between adjacent cells, sites that are aligned with regions within the venular basement membrane where there is lower deposition of certain BM constituents (Wang et al., 2006; Voisin et al., 2009, 2010). To further investigate the mechanisms and dynamics of neutrophil migration through the pericyte sheath, in this study we have used numerous imaging modalities (including three-dimensional [3D] real-time imaging) to analyze pericyte morphology and neutrophil–pericyte interactions in inflamed cremasteric venules. The results show that pericytes actively support neutrophil migration through venular walls and that blockade of neutrophil crawling on pericytes inhibits neutrophil transmigration. Specifically, we observed that neutrophils exhibited sub-EC crawling along pericyte processes to gaps between adjacent pericytes. The directionality and speed of this crawling response within venular walls, termed abluminal crawling, appeared to be supported by pericyte-expressed intercellular adhesion molecule-1 (ICAM-1) and its leukocyte integrin ligands, Mac-1 and LFA-1. Finally, we provide evidence for the ability of pericytes to exhibit shape change resulting in enhanced mean gap size between adjacent cells. These sites were preferentially used as exit points by transmigrating neutrophils in response to the proinflammatory cytokines TNF and IL-1β. This effect appeared to be mediated via direct stimulation of pericytes, as these cells were found to express receptors for both TNF and IL-1β. Collectively, the study identifies several modes through which pericytes support neutrophil migration through venular walls, adding additional steps to the leukocyte adhesion cascade that describes the process of leukocyte infiltration into inflamed tissues.

RESULTS

Four-dimensional (4D) imaging of neutrophil–pericyte interactions in vivo

To facilitate our studies, transgenic α*SMA-RFPcherry* mice were bred with *Lys-EGFP-ki* mice (Faust et al., 2000), resulting in the generation of a novel mouse colony that expressed RFPcherry pericytes and enhanced GFP (EGFP) neutrophils and monocytes. The application of confocal intravital microscopy (IVM) to analyze inflammatory events within cremasteric venules of these mice resulted in a uniquely powerful model for the study of neutrophil–pericyte interactions in real-time in three dimensions (Fig. 1, A and B; and Video 1). The image acquisition settings were optimized for tracking of GFP^{high} neutrophils, with GFP^{low} monocytes being barely visible (Woodfin et al., 2011). Furthermore, in vivo immunostaining of EC junctions using an anti–platelet EC adhesion molecule-1 (PECAM-1) mAb (clone 390, which was previously shown not to effect leukocyte transmigration; Christofidou-Solomidou et al., 1997; Woodfin et al., 2011) allowed for tracking of neutrophils through both the endothelium and pericytes (Fig. 1 C). The model enabled us to observe neutrophil behavior at different stages of their migration through venular walls and into the interstitial space (Fig. 1 C). In investigating TNF-stimulated tissues, the following steps were observed and analyzed: (a) migration of neutrophils through the endothelium (largely through EC junctions; trans-EC migration [TEM]); (b) crawling of neutrophils within the venular wall (abluminal crawling); (c) migration of neutrophils through gaps between adjacent pericytes; and (d) migration of leukocytes into the interstitial tissue (Fig. 1 D). Neutrophils were found to have distinct morphological profiles at these different steps, e.g., significant flattening, reduced sphericity, and reduced elongation when crawling within the venular wall (abluminal crawling), as compared with leukocytes exhibiting luminal crawling (unpublished data). These parameters enabled us to clearly identify and analyze the dynamics of neutrophil abluminal behavior after TEM and when in contact with the pericyte sheath.

Analysis of the dynamics of different transmigration steps showed that in response to TNF, neutrophils breached ECs rapidly (average duration of ∼4 min), which is in line with TEM dynamics observed when using other stimuli (Woodfin et al., 2011). After TEM, neutrophils exhibited significant venular wall (abluminal) crawling, covering an average distance of ∼54 µm within a period of 20 min before breaching the pericyte sheath by migrating through gaps between adjacent cells with a duration of 11.1 ± 0.8 min. Crossing the venular walls from the first captured frame showing a leukocyte entering an EC junction to an EC entering the interstitial space took ∼35 min. Overall, these results show the development of a uniquely powerful imaging method for direct observation of neutrophil–pericyte interactions in real time, enabling investigations of the profile, dynamics, and mechanisms of neutrophil migration through venular walls beyond TEM.

ICAM-1, Mac-1, and LFA-1 mediate neutrophil crawling on pericytes

The aforementioned imaging method was applied to a more in-depth investigation of neutrophil–pericyte interactions in 4D. Tracking neutrophils beyond TEM demonstrated that the motility of neutrophils within venular walls was governed by the morphology of pericytes in that leukocytes used pericyte processes as tracks for their crawling behavior (Fig. 2, Video 2, Video 3, Video 4, and Video 5). Although neutrophils crawled an average distance of 54.4 ± 3.9 µm on pericytes before breaching the pericyte layer, the displacement length covered (i.e., the minimum distance between the TEM site and the eventual pericyte gap used by neutrophils to breach the pericyte layer) was on average 17.3 ± 0.9 µm. The significant difference in the quantified total migration distance and straight displacement distance is accounted for by the meandering nature of this motility response within the curved venular wall (Fig. 2 C). In some instances, multiple neutrophils were

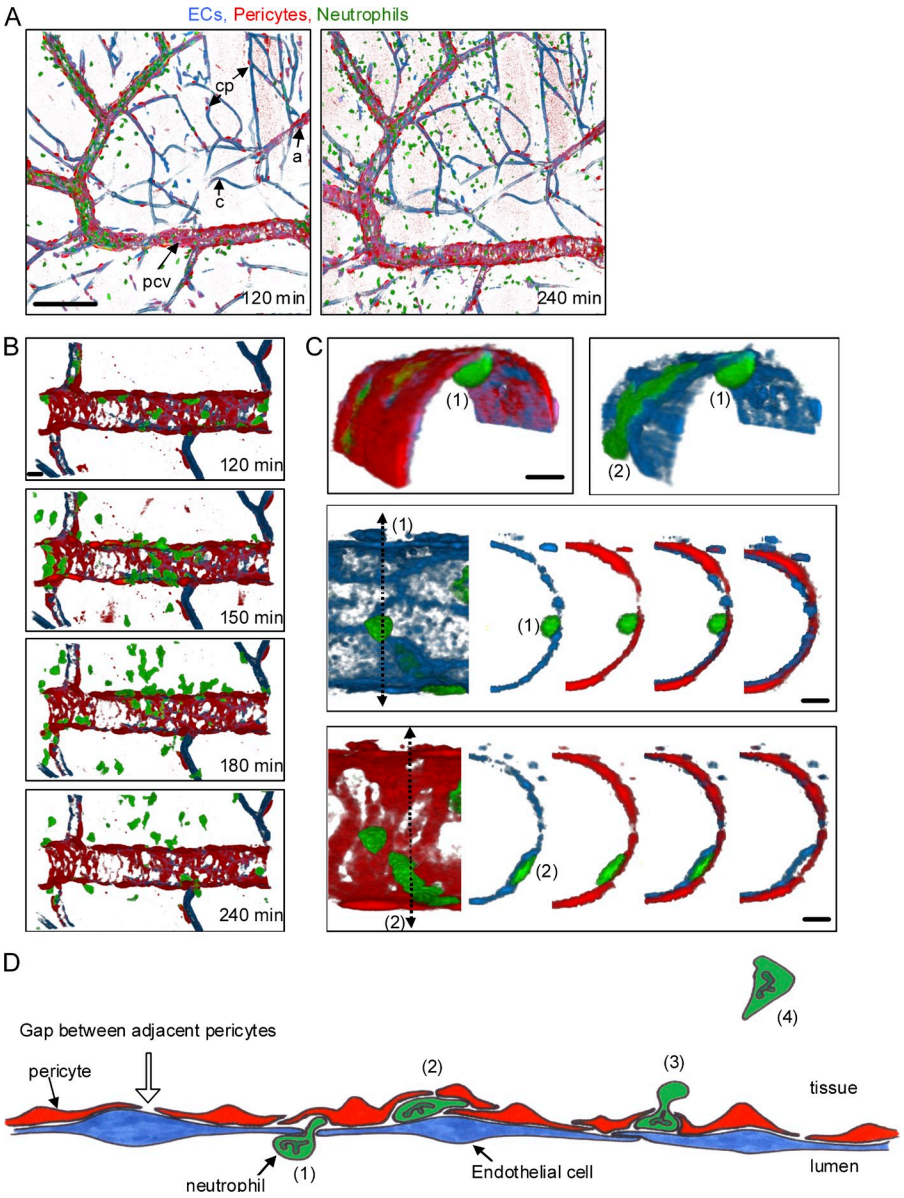

Figure 1. 4D imaging of neutrophil transmigration. α*SMA-RFPcherry* × *Lys-EGFP-ki* mice exhibiting endogenously labeled pericytes (*RFPcherry*, red) and neutrophils (*EGFP*, green) were subjected to EC junctional labeling using a directly conjugated Alexa Fluor 647 nonblocking mAb to PECAM-1 mAb (blue). (A) Composition of six 3D-reconstructed confocal images of the cremasteric microcirculation 120 and 240 min after intrascrotal injection of TNF. a, arteriole; c, capillary; cp, capillary pericyte; pcv, postcapillary venule. Bar, 100 µm. (B) Still images of a cremaster muscle postcapillary venule showing the development of an inflammatory reaction at the indicated time points after stimulation with TNF. Bar, 10 µm. (C) The images in the top panels are 3D reconstructions of half postcapillary venules showing a luminal neutrophil at an early stage of breaching the endothelium (cell 1) and a neutrophil that has already crossed the endothelium and is between the endothelium and pericyte layer (cell 2) at 3 h after TNF stimulation. The middle and bottom panels show the position of the indicated neutrophils from the luminal side (left hand side) or from 2-µm cross-sections of venules (right hand side) along the indicated lines demonstrating the position of the leukocyte relative to ECs and the pericyte layer. Bar, 10 µm. (D) Using the 3D real-time imaging model to analyze neutrophil transmigration through venular walls, several distinct steps were observed as illustrated in the diagram: (1) TEM, (2) motility between endothelium and the pericyte sheath (abluminal crawling), (3) migration through gaps between adjacent pericytes, and (4) interstitial migration. Images are representative of at least six separate experiments.

observed to be following each other within the venular wall to the same pericyte gap or along the same pericyte processes (see following paragraph). Interestingly, the majority of neutrophils tracked for abluminal crawling were seen to use pericyte processes as substrate (approximately >98%) and avoided gaps between adjacent pericytes (Fig. 2).

As neutrophil intravascular crawling is reportedly ICAM-1 and Mac-1 dependent (Phillipson et al., 2006), we hypothesized that abluminal neutrophil crawling on pericytes may also be mediated by similar mechanisms. In initial studies, we investigated the expression of ICAM-1 on venular pericytes in vivo. Immunostaining of fixed cremaster muscles for ICAM-1 indicated a significant up-regulation in the expression of this adhesion molecule on both ECs and pericytes of TNF-stimulated venules as compared with unstimulated tissues (Fig. 3, A and B). Furthermore, local administration of functional blocking anti–ICAM-1 mAb and anti–Mac-1 mAbs (injected 2 h after TNF stimulation) impaired neutrophil crawling on pericytes as compared with responses detected in control mAb-treated tissues (Fig. 3, C and D). Specifically, in anti–ICAM-1 mAb-treated cremaster muscles, abluminal neutrophils exhibited reduced speed and length of crawling within venular walls, resulting in cells occasionally "moving on the spot," (i.e., exhibiting multiple oscillatory movements without significant displacement [<1 cell diameter]). As ICAM-1 blockade led to an overall reduction in the displacement length covered by crawling neutrophils (Fig. 3 D), under these circumstances neutrophils breached the pericyte layer at sites closer to the site of TEM as compared with control antibody-treated animals. Overall, anti–ICAM-1 and anti–Mac-1 mAbs caused similar inhibitory effects on dynamics of neutrophil–pericyte interactions and significantly enhanced the total

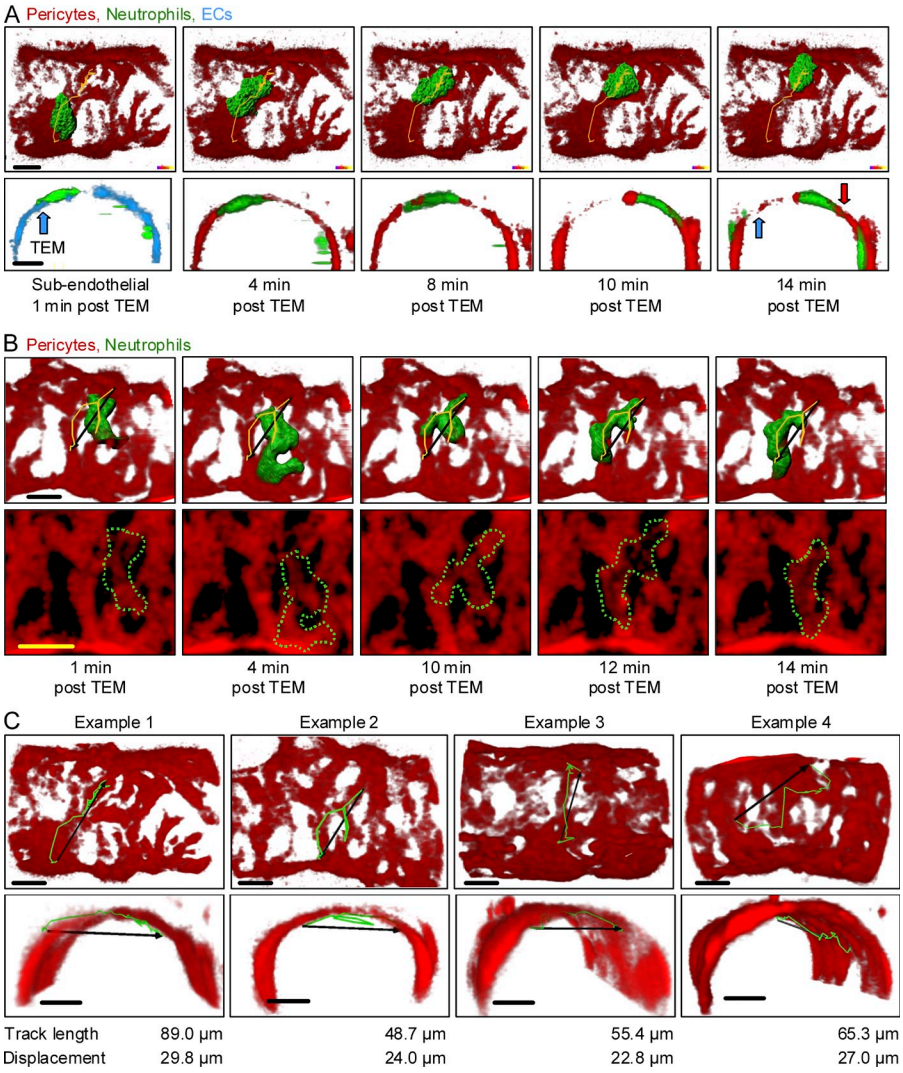

Figure 2. Analysis of neutrophil abluminal crawling in vivo. Cremaster muscles of αSMA-RFPcherry x Lys-EGFP-ki mice were stimulated with TNF for 2 h before being exteriorized and visualized by live confocal microscopy. (A) Time-lapse images showing a neutrophil (green) crawling along pericyte processes (red) from its site of TEM (i.e., starting point of the time course analysis, blue arrow) toward a gap between adjacent pericytes (red arrow). In the top panels, the neutrophil and pericyte layer are viewed from outside the vessel. The crawling path is shown with the yellow line. An isosurface mask was created to enable clearer visualization of the migrating neutrophil within the pericyte layer. In the bottom panels, 2-µm cross-sections in the z-axis show the position of the migrating neutrophil relative to the EC layer (blue) in the first image showing that it has passed the endothelium. The subsequent images show the neutrophil in relation to pericytes (red) during its abluminal crawling as captured at multiple time points. (B) Time-lapse images showing another example of neutrophil crawling along pericyte processes and avoiding the gaps between adjacent pericytes. Crawling path (yellow line) and directionality (black arrow) are shown in the top panels; the vessel segment is viewed in 3D from outside the vessel. The bottom panels show a higher magnification maximal intensity projection (2D) of the vessels with the shape of the neutrophil drawn with a green dotted line at each of the time points to illustrate its shape and its position relative to pericyte processes. (C) Four examples of postcapillary venules (pericyte in red) viewed in 3D from the extravascular space (top) or at a z-section angle (bottom), together with individual crawling paths (green line) and directionality (black arrow) of the neutrophil being tracked along pericyte processes in 3D. For clarity, the neutrophil being tracked is not depicted. Examples 1 and 2 show both the migration path and directionality of cells being tracked in A and B, respectively. All corresponding track and displacement lengths are given below the images. Bars, 10 µm.

abluminal duration of neutrophils as compared with control mAb-treated animals (mean duration of 29.4 ± 4.3, 47.5 ± 5.4, and 41.9 ± 3.6 min for tissues treated with control mAb, anti–ICAM-1 mAb, and anti–Mac-1 mAb, respectively; n = 5–8 mice per group; $P < 0.05$). An anti–LFA-1 mAb also exerted an inhibitory effect on the dynamics of neutrophil–pericyte interactions, although it appeared to be less efficacious than the anti–Mac-1 mAb (Fig. 3 D). The effects of all three mAbs on neutrophil crawling on pericytes correlated with reduced total neutrophil extravasation at 4 h after TNF stimulation (Fig. 3 E).

The protocol used for administering the blocking mAbs (i.e., local administration and 120 min after injection of TNF) did not affect early luminal neutrophil–EC adhesion (unpublished data) and thus enabled us to analyze the effects of the mAbs on neutrophil responses after TEM. Furthermore, to control for the potential Fc-mediated effects of the anti–ICAM-1 mAb, the effect of the pericyte binding anti-PDGFRβ mAb was tested in this assay and shown to have no impact on neutrophil crawling parameters or total neutrophil transmigration (unpublished data).

Because TNF-stimulated tissues showed enhanced levels of the chemokine KC on both ECs and pericytes (Fig. 3 F), the results suggest that pericyte-associated chemokines may trigger ICAM-1–dependent neutrophil crawling on pericytes through activation of integrins and directed migration through specific pericyte gaps. Collectively, the present findings report on the profile and mechanism of neutrophil crawling on pericytes, identifying this sub-EC crawling response as a distinct step in the cascade of adhesive events that mediate leukocyte transmigration in vivo.

Neutrophils migrate through enlarged pericyte gaps

The aforementioned findings indicated that neutrophil crawling on pericyte processes was prerequisite to leukocyte breaching

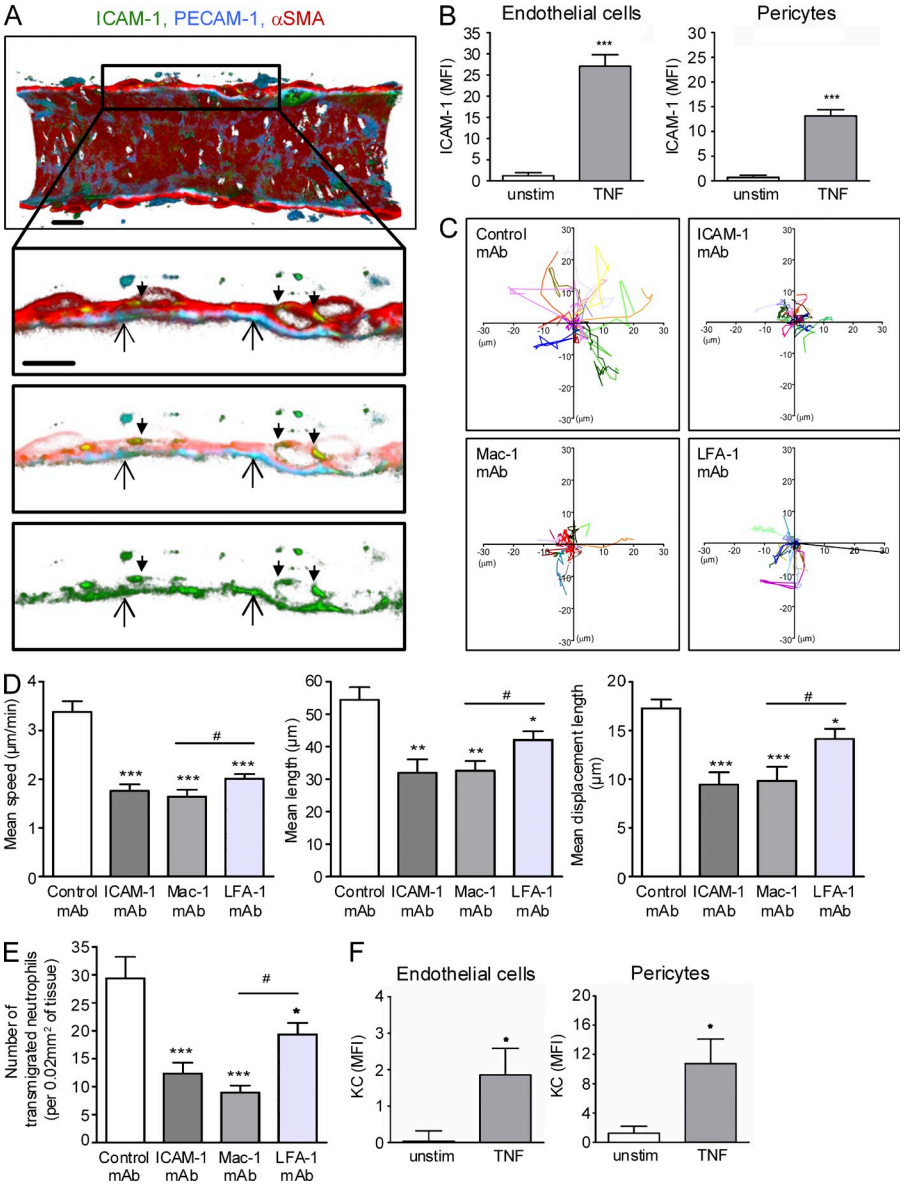

Figure 3. ICAM-1 and the integrins Mac-1 and LFA-1 mediate neutrophil–pericyte interactions. (A) Representative 3D-reconstructed confocal image of a TNF-stimulated (3 h) cremasteric postcapillary venule immunostained for PECAM-1 (EC, blue), ICAM-1 (green), and αSMA (Pericytes, red). The region within the box is enlarged in the images below following a longitudinal 2-μm cross-section of the vessel. In the middle panel of the enlarged region, a 4% opacity filter on the PECAM-1 and αSMA channels was applied to highlight ICAM-1 expression on the endothelium (arrow) and on the pericyte layer (arrowhead). The bottom panel shows only the ICAM-1 channel. Bars, 10 μm. (B) MFI per unit volume of ICAM-1 labeling on ECs and pericytes in unstimulated control and TNF-stimulated (3 h) tissues. (C) Effect of antibody blockade of ICAM-1, Mac-1, and LFA-1 on TNF-induced abluminal neutrophil crawling (after TEM) as observed in vivo in cremasteric postcapillary venules of using 4D confocal IVM. 2 h after intrascrotal injection of TNF in *αSMA-RFPcherry x Lys-EGFP-ki* mice (post-TEM migration), anti–ICAM-1, Mac-1, or LFA-1 blocking or isotype-matched control antibodies were injected i.s. for 30 min before cremasteric exteriorization. Crawling paths of abluminal neutrophils are shown (example of 20 per group for clarity) as normalized for their origins (sites of TEM). (D) Effect of anti–ICAM-1, Mac-1, and LFA-1 blocking antibodies on neutrophil abluminal crawling parameters as compared with control antibody-treated animals. The three graphs show the mean speed, total distance length, and displacement length of crawling. Data were obtained after analysis of a minimum of 211 crawling cells. (E) Number of extravasated neutrophils at 4 h after TNF stimulation of cremasteric muscles in animals treated with local injection of blocking anti–ICAM-1, Mac-1, and LFA-1 mAbs or isotope match control mAb. (F) MFI of KC staining per unit volume on ECs and pericytes in unstimulated control and TNF-stimulated (3 h) cremasteric venules. Results are expressed as mean of $n = 4$–5 vessels per mouse with at least 5 animals per group (A and B), 5–11 vessels from 4 animals (F), and from 1 vessel per animal with at least 6 animals/groups (C–E). Significant differences between groups are indicated by *, $P < 0.05$; **, $P < 0.01$; ***, $P < 0.001$. Significant differences between the anti–Mac-1 and anti–LFA-1 treated groups are indicated by # ($P < 0.05$).

of the pericyte layer. This response occurred via migration of neutrophils through gaps between adjacent pericytes, and pericyte transcellular migration was never noted in the present studies. Using our real-time 3D imaging platform, we observed that neutrophils did not, however, appear to breach the pericyte layer in a random fashion but in fact used certain gaps between adjacent pericytes preferentially (only 8.7 ± 1.3% of the total pericyte gaps were used from 6 venular segments analyzed in 6 animals). This resulted in the existence of noticeable hot spots, where multiple leukocytes were seen to exit the venular wall at the same site (Fig. 4, A and B; and Video 6), i.e., 28.9% of pericyte gaps used by neutrophils supported single transmigration events, whereas 59.7% of the gaps used were breached by multiple leukocytes (3 neutrophils on average, but in rare cases up to 9 neutrophils/pericyte gap was observed). To analyze the dynamics of this phenomenon in a quantitative manner, we analyzed the behavior of three neutrophils (termed cell 1, cell 2, and cell 3) migrating in a sequential manner through the same hot spot pericyte gap within multiple transmigration sequences. The results indicated that after TEM, the crawling velocity of cell 1 as compared with cell 3 was significantly slower (3.0 ± 0.2 vs. 4.0 ± 0.3 μm/min, respectively; $n = 127$ cells analyzed in 7 venules; $P < 0.01$), and the level of track straightness of cell 1 versus cell 3

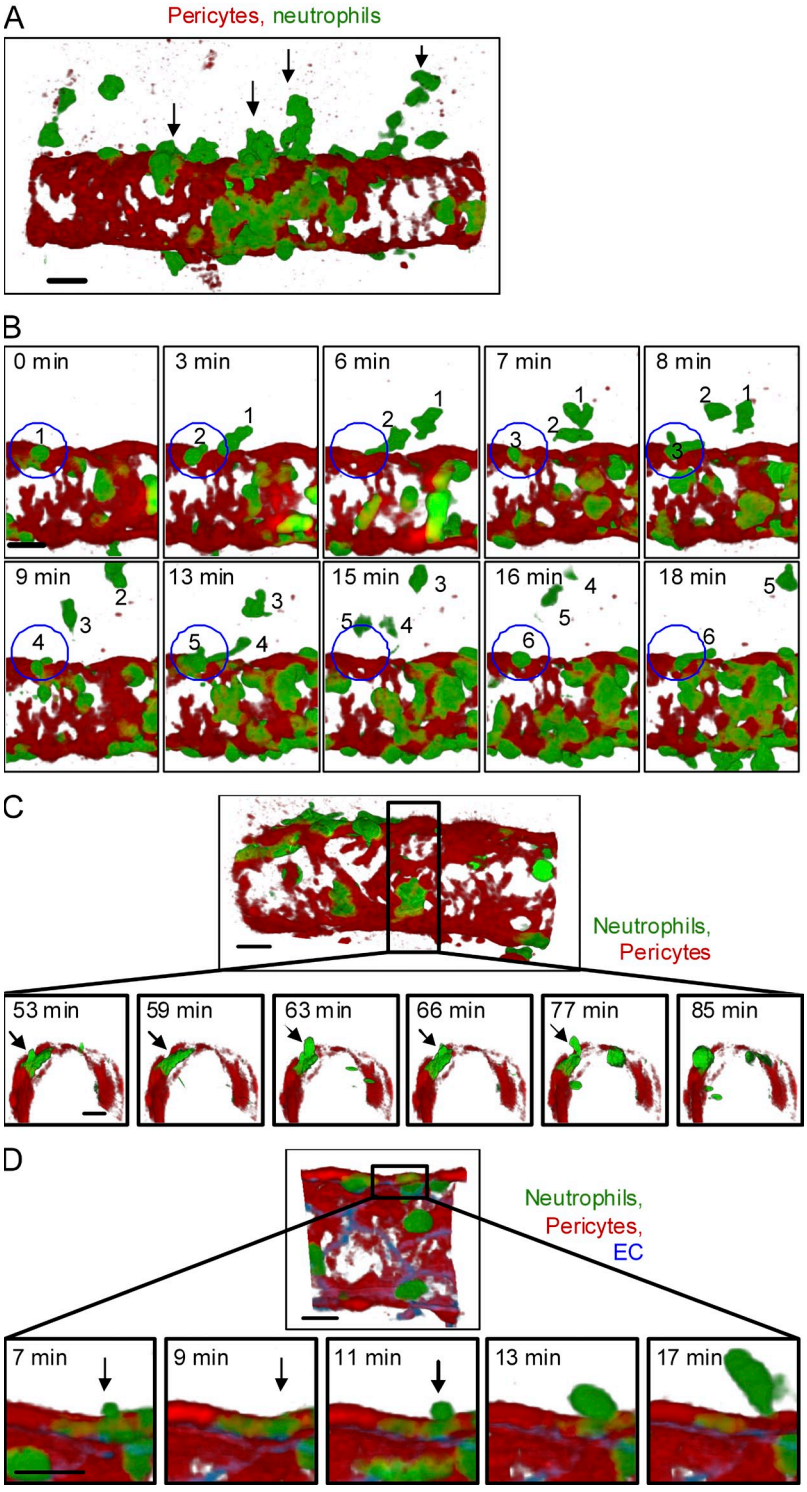

Figure 4. Migration of neutrophils through the pericyte sheath is site specific. (A) A representative 3D reconstructed image of TNF-stimulated cremasteric postcapillary venule from a αSMA-RFPcherry x Lys-EGFP-ki mouse (180 min after inflammation) illustrating the existence of sites in the venular wall that support the transmigration of multiple consecutive neutrophils (indicated by arrows). (B) Higher magnification images acquired at indicated time points illustrating the time course of migration of multiple neutrophils (labeled 1–6) through the same site within the pericyte layer (blue circles). The sequence of images initiates with the breaching of the pericyte layer by cell 1. (C and D) Two examples showing the ability of a neutrophil to exhibit hesitant transmigration through gaps in the pericyte sheath, i.e., exhibit multiple protrusions and/or oscillatory movements before finally breaching the pericyte layer from a TNF-stimulated cremaster muscle of an αSMA-RFPcherry x Lys-EGFP-ki mouse as observed by 4D confocal IVM. The top panels are images of a half cremasteric venule viewed from the luminal side (C) or extravascular space (D). The boxed regions show the transmigration of a neutrophil through the pericyte sheath at the indicated time points. The arrows indicate a neutrophil extending a protrusion toward the extravascular space that was then withdrawn once (C) or twice (D) after TEM before completing the extravasation response through the pericyte layer. All images are representative of at least $n = 6$ experiments (1 vessel/mouse, 1 mouse/experiment). Bar, 10 µm.

was significantly lower (0.32 ± 0.03 vs. 0.63 ± 0.08 µm/min, respectively; $P < 0.001$). Overall, it appears that neutrophils that follow other neutrophils to the same pericyte gap move toward the gap faster and with less meandering motility. Furthermore, the duration of neutrophil migration through the pericyte gap was significantly higher for cell 1 as compared with cell 3 (15.3 ± 1.6 vs. 5.9 ± 1. 7 µm/min, respectively; $P < 0.001$). These results suggest that neutrophils can follow each other through the same gaps within the pericyte layer and that when they do, the followers move faster and more directly to the exit points than the leaders. Interestingly, lead neutrophils often inserted multiple protrusions into pericyte gaps (in 24.2% of all observed transmigration events), and thus exhibited multiple oscillatory movements at different sites within the pericyte layer (hesitant breaching of pericytes) before deciding on their exit point (Fig. 4, C and D). This phenomenon was rarely seen with subsequent neutrophils that breached the same gap. This oscillatory phenomenon was increased in anti–ICAM-1 mAb-treated animals (24.2 vs. 66.7% for isotype control vs. anti–ICAM-1–treated tissues, respectively). These findings indicate that ICAM-1 blockade forces neutrophils to migrate toward undesirable pericyte gaps, resulting in greater frequency of hesitant (and hence slower) breaching of the pericyte layer.

As migrating through gaps between adjacent pericytes was a key step in penetrating the venular wall, we next investigated the possible association of this response with the size of the used gaps. Using real-time imaging, we quantified the average size of pericyte gaps used by transmigrating neutrophils

to be 21.3 ± 2.3 μm² at 2–4 h after TNF stimulation. However, neutrophils were able to migrate through a broad range of gap sizes (from 2.3 to 106 μm² in 105 pericyte gaps analyzed from 11 animals). Interestingly, analysis of tissues at 2 h after TNF stimulation indicated that 69.2 ± 5.6% of transmigration events occurred via pericyte gaps within the range of 8–50 μm². This accounted for 45.6 ± 2.2% of gaps in stimulated tissues and 32.1 ± 2.2% of gaps in unstimulated tissues (Fig. 5 A). In contrast, very few neutrophils (<4%) could be detected migrating through very large gaps (>50 μm²).

To understand why certain pericyte gaps were preferentially used by transmigrating neutrophils, the distribution of expression of KC and ICAM-1 on pericytes was analyzed. Specifically, the expressions of these molecules on the pericyte cell body and pericyte gap border regions (2 μm in width) were quantified in TNF-stimulated cremasteric venules. On average, a significantly greater expression of KC and ICAM-1 was detected on pericyte cell bodies than on pericyte gap borders (Fig. 5 B); an observation that is in line with the ability of pericyte processes to support neutrophil crawling. Interestingly, however, a small proportion of gaps expressed higher levels of KC and ICAM-1 (11.0 ± 4.0% and 12.4 ± 5.0%, respectively; n = 260–317 gaps analyzed in 8 venules from 3 mice) on pericyte gap borders than the average levels found on the pericyte body. These KC/ICAM-1 high–expressing border regions were largely (~72%) associated with pericyte gaps of 8–50 μm² in size, i.e., the preferred size range used by transmigrating neutrophils.

Although very likely multiple other parameters (e.g., distribution of stimulatory and adhesive molecules) may govern the route taken by neutrophils through the pericyte layer, the size of gaps appears to be one determining factor, and so regulation of this parameter in inflamed tissues was investigated in more detail.

Pericyte gaps are enlarged by proinflammatory cytokines

Pericyte shape change in cytokine-stimulated mouse cremaster muscles was investigated over long-term in vivo test periods and, in multiple vessels, in fixed whole-mount tissues immunostained for αSMA. Staining of tissues with this method indicated a loose and nonconfluent coverage of postcapillary venules by pericytes (Fig. 6 A), which is in line with our real-time imaging approach using α*SMA-RFPcherry* mice (Fig. 1 A) and our previous findings (Wang et al., 2006; Voisin et al., 2010). In TNF-stimulated tissues, venules exhibited notably enlarged gaps between adjacent pericytes. Similar results were obtained in the ear and also when using the cytokine IL-1β (Fig. 6 A). Quantitative analysis of confocal images showed significant enlargement of gaps between adjacent pericytes in cytokine-stimulated tissues (Fig. 6 B). In the cremaster muscle, intrascrotal injection of TNF (2-h test period) or IL-1β (4-h test period) elicited 81 and 79% increase in mean gap size between adjacent pericytes, respectively, as compared with control tissues. In line

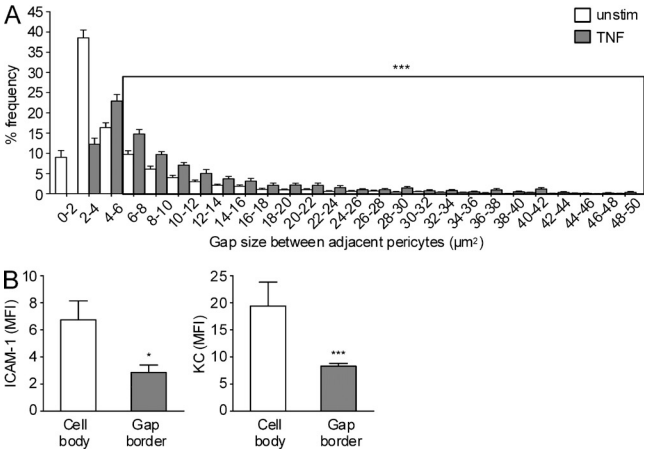

Figure 5. Neutrophils migrate through enlarged pericyte gaps. (A) The graph shows the frequency (percentage) of different sized gaps between adjacent pericytes in cremasteric postcapillary venules (unstimulated and TNF-stimulated) as detected by ex vivo immunofluorescence labeling and confocal microscopy. Gap sizes in the depicted range (1–52 μm²) represent ~97% of all detected gaps (at least 4 venules per animal analyzed in 5 mice). The boxed region indicates the range of gaps used by ~70% of observed transmigration events as analyzed by 4D confocal IVM (significantly different from the frequency of transmigration events detected in the nonboxed range; ***, P < 0.001). (B) Quantification of MFI per unit area of ICAM-1 (left) and KC (right) on pericyte cell body and at pericyte gap borders (a 2-μm wide region surrounding the gaps) after TNF-stimulation (3 h). Results are expressed as mean of at least n = 11 (A) and n = 5 (B) mice per group, respectively (with 3–4 vessels/cremaster, 2 cremasters/animal).

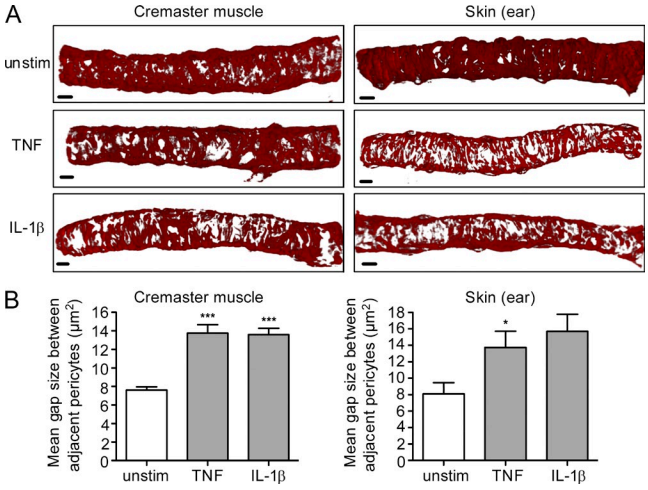

Figure 6. Effects of TNF and IL-1β on pericyte shape change in vivo. (A) WT mice were injected with either TNF or IL-1β for 2 or 4 h, respectively, into the cremaster muscle or intradermally in the ear. Tissues were then dissected away, fixed, and immunostained for the pericyte marker αSMA before being analyzed by confocal microscopy. Bars, 10 μm. (B) The graphs show the mean gap size between adjacent pericytes in unstimulated, TNF-, and IL-1β–stimulated venules of cremaster muscles (left) or the skin of the ear (right). Statistical significance between cytokine-stimulated tissues from the control group is indicated by asterisks. *, P < 0.05; ***, P < 0.001. Images are representative of n = 9 experiments (A) and results are expressed as mean of n = 7 mice per group (B; one mouse/experiment).

with our previous results (Wang et al., 2006;Voisin et al., 2009, 2010), no change in the number of pericyte gaps was noted in stimulated venules as compared with unstimulated tissues (unpublished data). This suggests that no new pericyte gaps are created and that neutrophils use existing, but in some cases enlarged, gaps for breaching the venular wall.

To complement the in vivo findings, pericyte responses were also investigated in vitro using the murine pericyte-like cell line C3H/10T1/2 (Reznikoff et al., 1973). For real-time analysis of C3H/10T1/2 responsiveness to TNF and IL-1β, cells were transfected with Lifeact-*EGFP* (Riedl et al., 2008), and changes in cell shape were imaged over a period of 4 h by fluorescence time-lapse microscopy (Fig. 7 A). Results showed a dose- and time-dependent change in cell elongation in response to both TNF and IL-1β (Fig. 7 B) caused by an increase in cell length and reduction in cell width. Under these circumstances, no change in total cell area was noted (unpublished data).

Collectively, these results demonstrate that pericytes can exhibit significant shape change both in vivo and in vitro in response to inflammatory cytokines, the former leading to enlarged gaps between adjacent cells in venules.

Pericyte shape change does not require neutrophils

In investigating the mechanism through which TNF and IL-1β induce pericyte shape change, we first sought to investigate if the observed responses were associated with the ability of TNF and IL-1β to induce neutrophil transmigration. To address this, in initial studies we analyzed the time course of pericyte shape change and neutrophil transmigration in TNF- and IL-1β–stimulated cremaster muscles as assessed by immunofluorescent staining and confocal microscopy of fixed whole-mount tissues. For this purpose, tissues were immunostained for αSMA (pericytes) and MRP-14 (neutrophils), as previously described (Fig. 8 A; Voisin et al., 2010). Locally applied TNF caused significant enlargement of gaps between adjacent pericytes at early time points (0.5 and 1 h), continuing to develop at 2 h (91% increase in mean gap size) and returning toward basal levels at 4 h (Fig. 8 B). IL-1β–induced pericyte shape change developed more slowly and was first detected at 4 h, after which it returned toward basal levels (Fig. 8 B). With both cytokines, the density of gaps (number of gaps/vessel area) was not altered at any time point investigated (unpublished data), suggesting an enlargement of preexisting gaps and not generation of new ones.

Although both TNF and IL-1β elicited pericyte shape change and neutrophil transmigration in a time-dependent manner, the temporal association of these responses appeared to differ for the two cytokines. Specifically, although in TNF-stimulated tissues pericyte shape change preceded neutrophil transmigration, the time course of pericyte shape change and neutrophil transmigration as induced by IL-1β were very similar (Fig. 8 B). To conclusively address the role of neutrophils in cytokine-stimulated pericyte shape change, responses induced by TNF and IL-1β in cremasteric venules of neutrophil-depleted mice were investigated. Both cytokines induced significant enlargement of gaps between adjacent pericytes in venules of control and neutrophil-depleted animals with no significant difference being observed between the two groups (Fig. 8 C). Collectively, the results indicate that TNF and IL-1β can induce pericyte shape change independently of neutrophil transmigration.

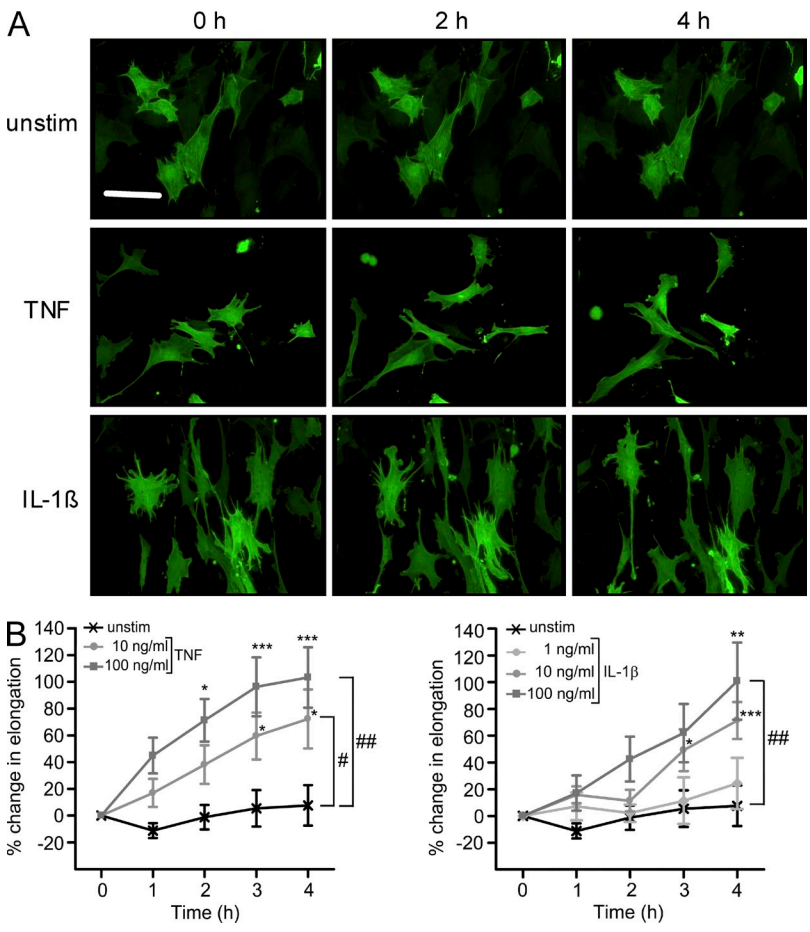

Figure 7. TNF and IL-1β stimulate shape change of pericyte-like C3H/10T1/2 cells in vitro. (A) Representative fluorescence time-lapse microscopy images of Lifeact-EGFP transfected C3H/10T1/2 cells are shown for the indicated time points after cytokine (2 and 4 h) or vehicle control (PBS, unstimulated group). The 0 h time point was captured before cytokine or PBS addition. Bar, 100 µm. (B) Graphs show the percentage change in cell elongation over time in response to different concentrations of TNF (left) or IL-1β (right). Data were obtained after analysis of a minimum of seven independent experiments. Statistical significance between each time point after stimulation and the unstimulated condition (0 h time point) are indicated by asterisks. *, $P < 0.05$; **, $P < 0.01$; ***, $P < 0.001$. Statistical significances between cytokine-stimulated (4 h) conditions and PBS-treated groups are indicated by hash symbols. #, $P < 0.05$; ##, $P < 0.01$. Images and results are from $n = 5$ experiments.

Pericytes express TNF and IL-1β receptors

To further address the mechanism through which TNF and IL-1β stimulate pericyte shape change, we investigated the potential expression of receptors for these cytokines on pericytes. Whole-mount cremaster muscles were immunostained for PECAM-1 (ECs), αSMA (pericytes), and TNFRI, TNFRII, or IL-1RI. Our results showed that ECs and pericytes expressed comparable levels of all three cytokine receptors

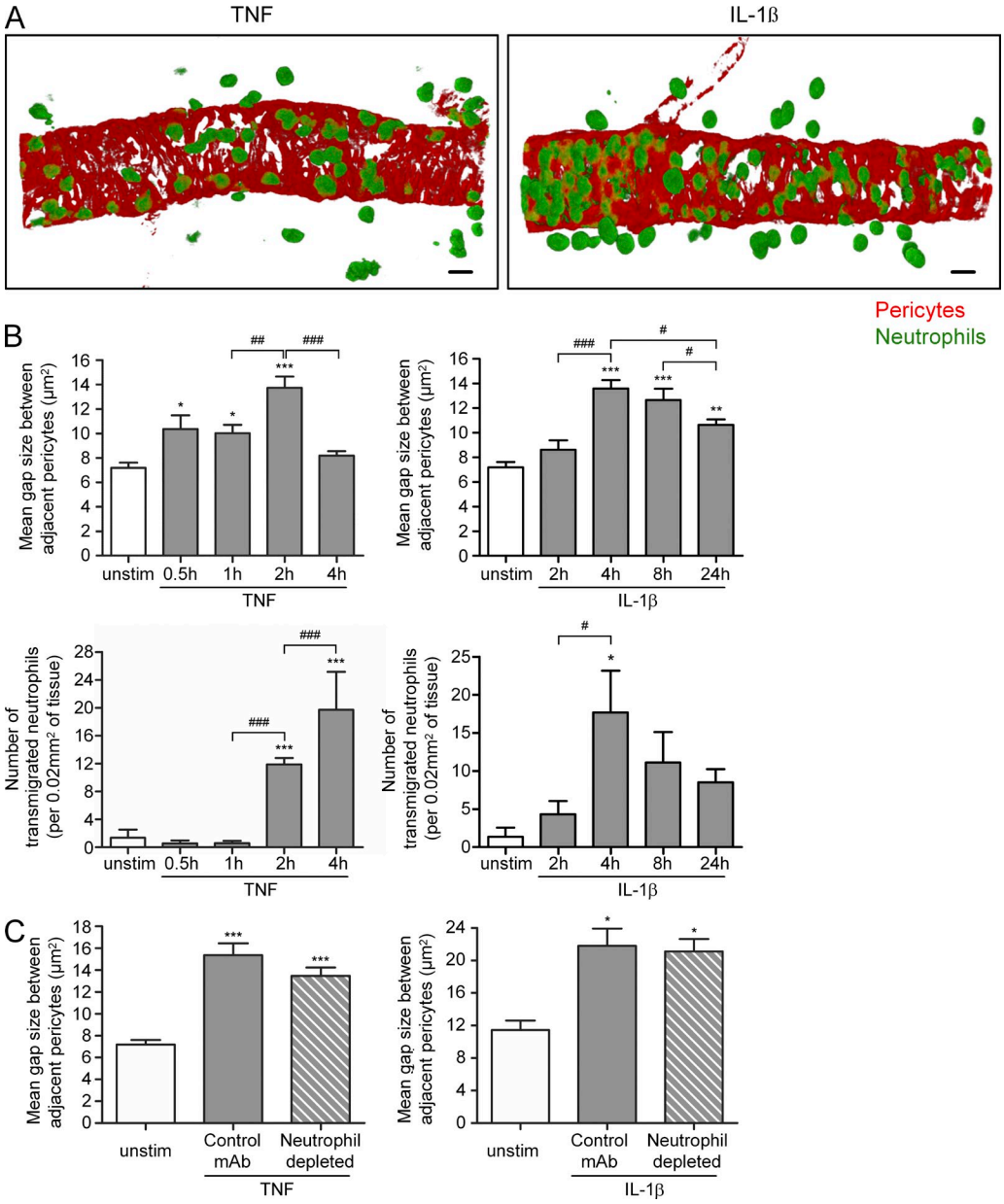

Figure 8. Cytokine-induced pericyte shape change can occur in a neutrophil-independent manner. TNF or IL-1β were injected i.s. into WT C57BL/6 mice and cremaster muscles were dissected at different time points after stimulation, fixed, immunostained for pericytes (αSMA, red) and neutrophils (MRP-14, green) and analyzed by confocal microscopy. (A) Representative images from TNF- (left) and IL-1β–stimulated (right) cremasteric venules illustrating the neutrophil infiltration responses obtained at the 4-h time point. Bars, 10 µm. (B) Time course of cytokine-induced increase in mean gap size between adjacent pericytes (top) and neutrophil transmigration (bottom) in response to TNF- (left) and IL-1β–(right). Statistically significant cytokine-induced responses, as compared with responses noted in unstimulated tissues, are indicated by *asterisks. *, $P < 0.05$; **, $P < 0.01$; ***, $P < 0.001$. Significant differences between responses at different time points are indicated by hash symbols. #, $P < 0.05$; ##, $P < 0.01$; ###, $P < 0.001$. (C) WT mice were depleted of their circulating neutrophils using an anti-GR1 antibody (100 µg, i.p.) 24 h before i.s. injection of TNF or IL-1β. Control mice were treated with an isotype control antibody. Mean size of pericyte gaps was quantified at 2 h (TNF) or 4 h (IL-1β) after stimulation. Significant differences from unstimulated controls are indicated by asterisks. *, $P < 0.05$; ***, $P < 0.001$. $n = 3–4$ experiments for (at least 4 vessels analyzed per animal per experiment).

(Fig. 9, A and B). The pericyte-like cell line C3H/10T1/2 cells also expressed all three cytokine receptors (Fig. 9 C). Collectively, these results demonstrate that pericytes express receptors for TNF and IL-1β, findings that can account for the observed pericyte shape change induced by these cytokines in vitro and in vivo.

DISCUSSION

Pericytes form an integral component of all blood vessels but, due to a lack of well accepted protocols for their isolation and culture, and availability of unequivocal pericyte markers, very little attention has been paid to investigations of leukocyte interactions with these mural cells. To address this fundamental issue, we have investigated the profile, dynamics, and mechanisms of leukocyte–pericyte interactions in inflamed tissues in vivo using an IVM platform with high spatiotemporal resolution. The findings report on previously unidentified modes by which pericytes facilitate leukocyte transmigration through venular walls, highlighting the need for further exploration of the role of pericytes under both physiological and pathological inflammatory conditions.

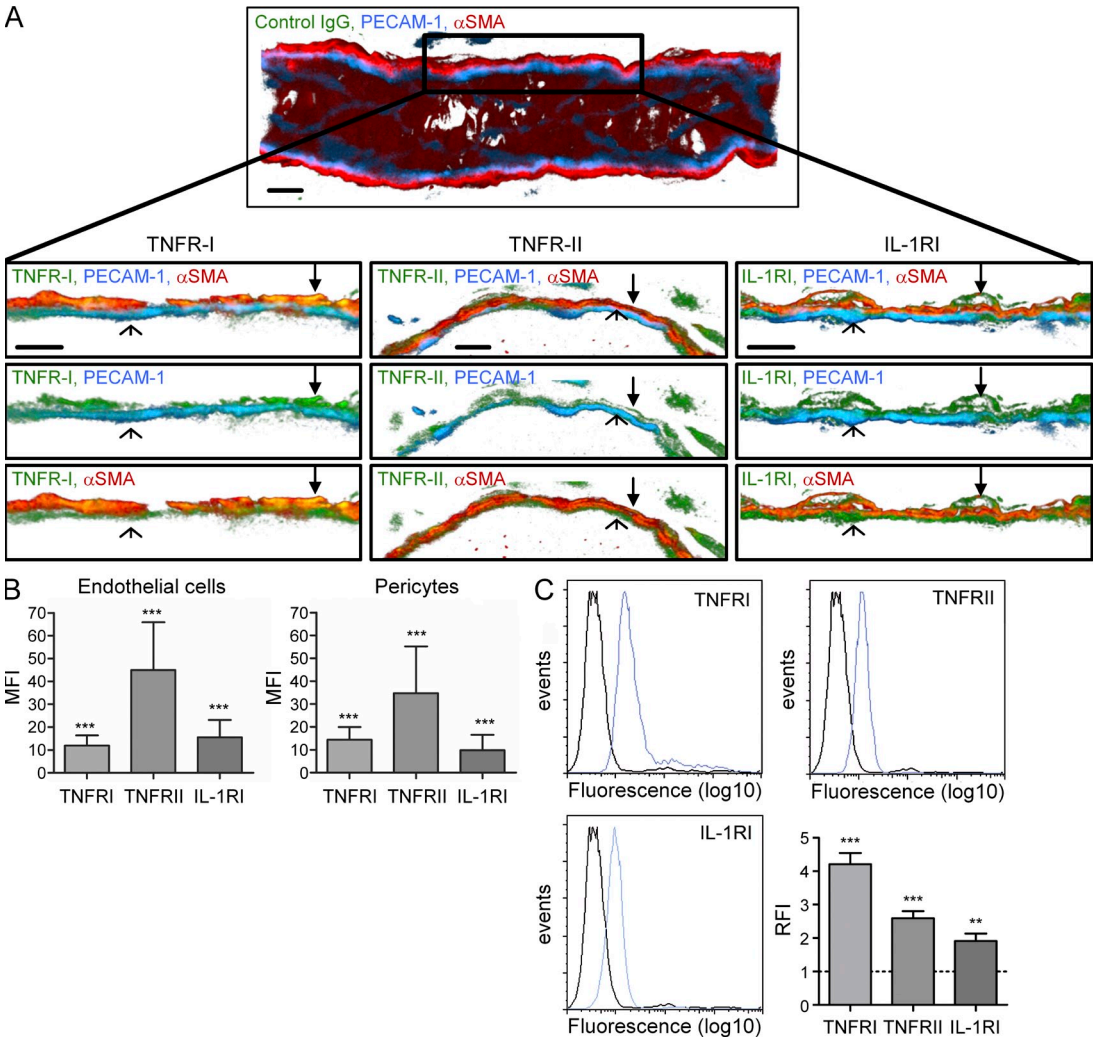

Figure 9. Pericytes express receptors for TNF and IL-1β. (A) The panels show a 3D-reconstruced postcapillary venule of an unstimulated cremaster muscle immunostained for PECAM-1 (EC junction, blue), αSMA (pericytes, red), and the cytokine receptor of interest (green) or with an isotype control antibody (top). A 1-µm-thick section of the dotted boxed region is enlarged below highlighting the specific expression of TNFRI, TNFRII, and IL-1RI on both ECs (black arrows) and pericytes (arrowhead). Bars, 10 µm. (B) Graphs show the MFI of TNFRI-, TNFRII-, or IL-RI–specific staining on ECs (left) and pericytes (right) as determined by IMARIS software. Significant expression of the cytokine receptors as compared with the binding of an isotype control antibody (Student's *t* test) is indicated by asterisks. ***, $P < 0.001$. (C) Representative flow cytometry histograms illustrate the presence of TNFRI, TNFRII, and IL-1RI on C3H/10T1/2 cells in vitro. Binding of isotype control antibodies (back lines) and primary mAbs directed against cytokine receptors (blue line) are shown as overlays. The graph (bottom right) shows mean RFIs for TNFRI, TNFRII, and IL-1RI. The dotted line indicates the isotype control RFI. Significant differences compared with the isotype control (Student's *t* test) are indicated by asterisks. *, $P < 0.05$; ***, $P < 0.001$. Representative images and results are from $n = 4$ mice (A and B; at least 3 vessels per mouse) and 6 (C) experiments.

To enable direct analysis of neutrophil–pericyte interactions, we applied confocal IVM to observations of events within the microcirculation of inflamed cremaster muscles of α*SMA-RFPcherry* transgenic mice crossed with *Lys-EGFP-ki* mice. The resultant mouse colony expressed red pericytes and green leukocytes, and thus provided a uniquely powerful tool for analysis and investigations of leukocyte–pericyte interactions. The imaging platform was optimized for tracking neutrophils (as opposed to monocytes) and also incorporated a highly effective mode of in vivo immunolabeling of EC junctions (Woodfin et al., 2011). This approach allowed investigations of neutrophil behavior and dynamics at different steps of the transmigration response, initiating with TEM and finishing with breaching of the pericyte sheath. The application of this technique to the analysis of TNF-stimulated tissues in 3D revealed that neutrophils could breach the endothelium rapidly, largely via a paracellular route (average duration, ∼4 min), in line with our previous findings with multiple other inflammatory reactions (Woodfin et al., 2011). After TEM, neutrophils exhibited a significant crawling response within the pericyte layer lasting ∼30 min and covering distances of ∼54 µm before crossing the pericyte sheath and entering the adjacent interstitial tissue. This abluminal crawling occurred in a highly meandering manner and crawling neutrophils clearly used pericyte processes as tracks. Indeed, neutrophil crawling was rarely seen in regions deficient of pericytes, i.e., within gaps between adjacent pericytes, suggesting a role for these mural cells in regulation of neutrophil motility within venular walls.

In investigating the adhesive mechanisms that support neutrophil–pericyte interactions, a role for ICAM-1 (on pericytes) and the integrins Mac-1 and LFA-1 (on neutrophils) was identified. Specifically, local application of blocking mAbs reduced the speed, track length, and displacement of neutrophil abluminal crawling in TNF-stimulated tissues. These effects were directly in line with enhanced duration of neutrophils within the venular wall and/or reduced neutrophil transmigration into the surrounding tissue, collectively suggesting a key role for neutrophil–pericyte interactions in regulation of neutrophil transmigration. Furthermore, TNF-stimulated tissues exhibited enhanced levels of ICAM-1 and the chemokine KC on both ECs and pericytes as compared with unstimulated tissues. These results indicate that, as found with ECs (Phillipson et al., 2006), neutrophil crawling on pericytes is driven by pericyte-expressed chemokines and ICAM-1. ICAM-1 has also previously been reported on TNF-stimulated human brain pericytes (Verbeek et al., 1995) and, more recently, on both unstimulated and cytokine-stimulated human placental pericytes (Maier and Pober, 2011), although its in vivo functional role had not previously been explored. As the inhibitory effect of the anti–ICAM-1 mAb on abluminal neutrophil crawling was partial, other pericyte-associated adhesion molecules may also contribute to this phenomenon. In this context, cultured human pericytes have been reported to express VCAM-1, but not ICAM-2 or E-selectin (Maier and Pober, 2011). Although pericyte-expressed VCAM-1 appears to support T cell adhesion in vitro (Verbeek et al., 1995), at present nothing is known about the role of pericyte VCAM-1 in vivo. Finally, although our findings provide evidence for the ability of pericyte ICAM-1 to support neutrophil abluminal crawling, we cannot rule out the possibility that ICAM-1 may also be abluminally expressed on ECs, and as such may have contributed to the ICAM-1–dependent neutrophil abluminal crawling reported here.

We observed that neutrophils following other neutrophils along pericyte processes exhibited markedly reduced meandering motility within venular walls, indicating that the slow and wandering first line neutrophils provided some directional cues and or paved the way for the followers. The resultant effect of this phenomenon was that clear hot spots were noted where multiple neutrophils were seen to exit venular walls through the same pericyte gap. Although preferred sites of neutrophil migration through the endothelium and the venular basement membrane have previously been reported (Burns et al., 1997; Wang et al., 2006; Voisin et al., 2009, 2010; Sumagin and Sarelius, 2010), the present findings are the first to report this phenomenon with respect to breaching the pericyte layer in real time. Potential mechanisms through which leading neutrophils may facilitate migration of the followers within the venular wall include release of chemoattractants, such as chemokines and lipid mediators, from the leading cells, or paving the way through the venular basement membrane. The latter may occur in a protease-dependent manner, a process that, in addition to remodeling the basement membrane, may also lead to generation of basement membrane–derived chemotactic molecules (Steadman et al., 1993; Wang et al., 2005, 2006; Pham, 2006; Mydel et al., 2008).

Crawling neutrophils eventually exited the venular wall through gaps between adjacent pericytes and, in contrast to a previous study (Feng et al., 1998), no transcellular pericyte breaching was observed in our models. We have previously reported that gaps between adjacent pericytes are colocalized with regions within the venular basement membrane, where lower levels of certain basement membrane constituents, such as collagen type IV, laminin-8, and laminin-10, exist. These sites, termed low expression regions (LERs), are preferentially used by transmigrating neutrophils and monocytes (Wang et al., 2006; Voisin et al., 2009, 2010). Interestingly, LERs are rich in perlecan (Voisin et al., 2010), a basement membrane constituent that is antiadhesive for neutrophils in vitro (Sixt et al., 2001), a phenomenon that may contribute to lack of neutrophil crawling on gaps between adjacent pericytes. In the present study, we show that only ∼9% of the gaps present within the pericyte sheath are used by transmigrating neutrophils. Furthermore, transmigrating leukocytes appeared to preferentially use enlarged pericyte gaps in that ∼70% of all the migratory events quantified occurred through gaps of 8–50 μm^2 in size. These accounted for ∼50% of gaps in inflamed tissues and ∼30% of gaps in unstimulated tissues. A key question raised by these findings is what are the determinants that govern the preferential use of certain gaps during neutrophil transmigration? As it has previously been shown

that ICAM-1 enrichment is associated with preferential leukocyte TEM through tricellular EC junctions (Sumagin and Sarelius, 2010), we sought to analyze the distribution of KC and ICAM-1 on pericytes in relation to different size gaps. In this context, our results indicated that, on average, the pericyte cell body expressed higher levels of KC and ICAM-1 than pericyte regions that acted as borders to gaps between adjacent cells. These findings are in line with our observations that pericytes support effective neutrophil crawling in a chemokine- and ICAM-1–dependent manner, with almost no crawling being seen on pericyte-deficient regions. Interestingly however, a small number of gaps (~10%) were bordered by pericyte regions expressing higher levels of KC and ICAM-1 than the average cell body levels. Furthermore, >70% of these "KC/ICAM-1 high" borders were associated with pericyte gaps of 8–50 μm^2 size, a gap size range preferentially used by transmigrating neutrophils. These associations suggest that expressions of KC and/or ICAM-1 near pericyte gaps may guide neutrophils to exit sites within the pericyte sheath. Although this presents a tantalizing possibility, at present we are unable to confirm this hypothesis in real-time neutrophil-tracking studies because of the lack of availability of a nonblocking anti–ICAM-1 mAb that can be used for in vivo labeling of pericyte ICAM-1.

Pericytes are contractile cells and, as such, several studies have shown the ability of pericytes to exhibit shape change after stimulation with vasoactive mediators in vitro, such as histamine (Murphy and Wagner, 1994; Speyer et al., 1999). As pericyte shape change appeared to facilitate neutrophil migration through the pericyte sheath, this response was investigated in more detail. Cremaster muscles or ear skin stimulated with TNF and IL-1β showed significantly enlarged gaps between adjacent pericytes, increasing by ~80% after a 2–4-h stimulation. Full time course analysis of pericyte shape change and neutrophil transmigration indicated that in response to TNF, the former preceded the response of neutrophil transmigration, suggesting that pericyte shape change occurs independently of neutrophils. This is in contrast to inflammation-induced remodeling of BM permissive regions (LERs), a response that we have previously shown to be strictly neutrophil dependent (Voisin et al., 2009, 2010; Wang et al., 2006). The ability of pericytes to exhibit shape change in a neutrophil-independent manner was conclusively demonstrated in studies where TNF and IL-1β were found to induce enlarged pericyte gaps in both control and neutrophil-depleted animals. To investigate the mechanism of this response, the potential expression of receptors for TNF and IL-1β on pericytes was explored. Immunofluorescence staining of unstimulated cremaster muscles revealed significant levels of TNFRI, TNFRII, and ILRI on pericytes comparable to levels detected on ECs. Parallel experiments conducted with the pericyte-like cell line C3H/10T1/2 (Reznikoff et al., 1973) showed the ability of these cells to exhibit change in morphology in response to TNF and IL-1β and to express TNFRI, TNFRII, and ILRI. Collectively, the present results demonstrate that pericytes express receptors for TNF and IL-1β and that activation of these receptors can lead to increased expression of ICAM-1 and KC that support neutrophil abluminal crawling after TEM to preferred pericyte gaps. However, our results show that pericyte shape change as induced by TNF and IL-1β in vivo can contribute to the generation of enlarged gaps between adjacent pericytes that are preferentially used by transmigrating neutrophils. Details of the signaling pathways that regulate pericyte shape change in vivo are at present unclear, but both TNF and IL-1β are known to activate small GTPases that play a key role in actin cytoskeleton rearrangement (Puls et al., 1999), and both cytokines have previously been reported to induce morphological changes in rat lung pericytes in vitro (Kerkar et al., 2006). In addition, the disassembly of αSMA stress fibers in isolated bovine retina pericytes causing reduced cell size in vitro is reportedly mediated via the small GTPase RhoA (Kolyada et al., 2003; Kutcher et al., 2007; Kutcher and Herman, 2009), but the potential role of such pathways in vivo has yet to be clarified.

In summary, through development of an imaging platform that allows direct quantitative analysis of neutrophil–pericyte interactions, we have unraveled several modes through which pericytes can facilitate neutrophil transmigration through venular walls. Hence, in addition to their accepted role in regulation of vascular tone, integrity, and barrier function (Shepro and Morel, 1993; Hirschi and D'Amore, 1996; Edelman et al., 2006), the present results demonstrate a role for pericytes in inflammation, indicating the need for further analysis of the role of these mural cells in vascular functions.

MATERIALS AND METHODS

Reagents. Recombinant murine TNF and IL-1β were purchased from R&D Systems. The neutrophil-depleting monoclonal rat anti–mouse Ly-6G and Ly-6C (GR1) antibody (clone RB6-8C5, NA/LE) was purchased from BD. The following primary antibodies were used for immunofluorescence labeling for confocal imaging and confocal IVM: monoclonal mouse anti–mouse αSMA-Cy3 (clone 1A4; Sigma-Aldrich); monoclonal rat anti–mouse ICAM-1 (clone YN1/1.4.7; eBioscience); monoclonal rat anti–mouse PDGFRβ (clone APB5), anti–mouse Mac-1 (clone M1/70), and anti–mouse LFA-1 (clone M17/4; BioLegend); monoclonal Armenian hamster anti–mouse IL-1RI (clone JAMA-147 used for flow cytometry; BioLegend); polyclonal goat anti–mouse IL-1RI (used for confocal microscopy; R&D Systems); monoclonal rat anti–mouse MRP-14 (clone 2B10; a gift from N. Hogg, Cancer Research UK, London, UK; Hobbs et al., 2003); nonblocking monoclonal rat anti–mouse PECAM-1 (clone C390; generated as described in Christofidou-Solomidou et al., 1997) directly conjugated to Alexa Fluor 647 using Molecular Probes Alexa Fluor Monoclonal Antibody Labeling kit (Invitrogen); monoclonal Armenian hamster anti–mouse TNFRI (clone 55R-286 used for flow cytometry; BioLegend); polyclonal goat anti–mouse TNFRI (used for confocal microscopy; R&D Systems); monoclonal Armenian hamster anti–mouse TNFRII (clone TR75-89 used for flow cytometry; BioLegend); polyclonal goat anti–mouse TNFRII (used for confocal microscopy; R&D Systems); rat anti–mouse KC (clone 124014 used for confocal microscopy; R&D Systems). The following purified antibodies were used as isotype-matched controls: Armenian hamster IgG_1 (BD), goat IgGs (R&D Systems), mouse IgGs (BD), or rat IgG2a or IgG2b (AbD Serotec). Appropriate secondary antibodies conjugated with Alexa Fluor dyes (Invitrogen) or biotin (BioLegend) were used if necessary. The biotinylated anti–Armenian hamster secondary antibody was detected using streptavidin conjugated with Alexa Fluor 488 (Invitrogen).

Animals. Male (20–25 g) mice from several colonies were used in this study. Pure WT C57BL/6 mice were purchased from Harlan-Olac. The α*SMA-RFPcherry* mice are transgenic animals in which the RFP variant cherry transgene was inserted and expressed upon the αSMA promoter, resulting in red fluorescent pericytes and smooth muscle cells. This mouse strain is on a C57BL/6 background and was generated according to established protocols previously detailed for generation of α*SMA-EGFP* transgenic mice (Yokota et al., 2006). The expression of RFPcherry was largely as found in the α*SMA-EGFP* transgenic animals. In brief, the regulatory sequence of αSMA gene promoter used contains −1,074 bp of the 5′ flanking region, the transcription start site, 48 bp of exon 1, the 2.5-kb intron 1, and the 15-bp exon 2 of mouse αSMA (Wang et al., 1997). This sequence was fused with the sequence of the red fluorescent protein RFPcherry (Shaner et al., 2004). Transgenic DNA purification and microinjection of the DNA were performed as described previously (Schlaeger et al., 1995). The *Lys-EGFP-ki* mice (backcrossed on C57BL/6 background for at least 8 generations; Faust et al., 2000), in which the gene for EGFP has been knocked into the lysozyme M (lys) locus, exhibit fluorescent myelomonocytic cells, with mature neutrophils comprising the highest percentage of EGFP high cells. These mice were used with the permission of T. Graf (Albert Einstein College of Medicine, Bronx, NY) and were provided for the study by M. Sperandio (Ludwig Maximilians University, Munich, Germany). Finally, the novel α*SMA-RFPcherry* × *Lys-EGFP-ki* mouse strain was generated in-house by interbreeding the α*SMA-RFPcherry* transgenic mice with *Lys-EGFP-ki* animals, yielding a valuable mouse colony expressing red pericytes and green leukocytes (neutrophils and monocytes) that were used for real-time confocal microscopy technique. Only mice heterozygote for *Lys-EGFP-ki* that showed normal transmigration responses in vivo (Woodfin et al., 2011) were used in the study, and thus no other littermates or WT mice were needed as controls. All animals were housed in individually ventilated cages and facilities were regularly monitored for health status and infections. All experiments were performed under the UK legislation for the protection of animals, and at the end of all in vivo procedures involving anesthesia, animals were humanely killed by cervical dislocation in accordance with UK Home Office regulations.

Induction of inflammatory reactions in the murine cremaster muscle. The cremaster muscle was used as the principal tissue for analysis of leukocyte–vessel wall interactions because of its thin and transparent nature, which allows it to be whole mounted for immunofluorescence staining and confocal microscopy. For this purpose, mice were sedated via intramuscular (i.m.) injection of 1 ml/kg anesthetics (40 mg ketamine and 2 mg xylazine in saline), and subsequently stimulated locally via intrascrotal (i.s.) injection of TNF (300 ng/400 µl saline) or IL-1β (50 ng/400 µl saline). As vehicle control, mice received i.s. injection of 400 µl saline. Different in vivo test periods were investigated as governed by the time course of action of these stimuli and the experimental objective. At the end of the in vivo test periods, mice were either sacrificed and cremaster muscles were dissected away and fixed for subsequent ex vivo analysis using immunofluorescence labeling and confocal microscopy, or mice were anaesthetized via i.p. injection of ketamine (100 mg/kg) and xylazine (10 mg/kg) in saline. Cremasters were surgically exteriorized for in vivo analysis using confocal IVM, as previously described (Woodfin et al., 2011).

Induction of inflammatory reactions in the mouse ear skin. Pure C57BL/6 animals were sedated and injected intradermally (i.d.) with TNF (150 ng/30 µl PBS), IL-1β (10 ng/30 µl PBS), or 30 µl PBS (vehicle control) in the ear. At the end of the experiments, mice were sacrificed and ears were dissected away for subsequent ex vivo analysis by immunofluorescence labeling and confocal microscopy, as previously described (Voisin et al., 2010).

Neutrophil depletion. Pure C57BL/6 mice were depleted of their circulating neutrophils by i.p. injection of anti-GR1 antibody (100 µg/1 ml saline) 24 h before i.s. administration of TNF or IL-1β. Control mice received the rat IgG2b isotype-matched control antibody. To determine the level of neutrophil depletion, blood neutrophil counts were performed as previously described (Wang et al., 2006). In brief, tail vain blood samples were collected before and 24 h after antibody administration, indicating an average neutrophil depletion of >80%. This almost total depletion of neutrophils in GR1-treated mice was also confirmed by confocal microscopy analysis of TNF-stimulated cremaster muscles stained for MRP-14 (neutrophil marker).

Immunofluorescence labeling and confocal microscopy analysis of whole-mounted murine tissues. Pure C57BL/6 mice were sacrificed and cremaster muscles or ears were dissected away and fixed in 100% methanol or 4% paraformaldehyde (PFA) in PBS for 30 min at 4°C. Subsequently immunofluorescence staining and confocal analysis of whole mounted tissues was performed as previously described (Voisin et al., 2010). In brief, to visualize pericytes (anti-αSMA antibody) and/or neutrophils (anti–MRP-14 antibody) and the cytokine receptors IL-1RI, TNFRI, TNFRII, and the chemokine KC, tissues were blocked and permeabilized in PBS containing 10% normal goat serum or rabbit serum (depending on the species of secondary antibodies used), 10% FCS, and 0.5% Triton X-100 for 2 h at room temperature. This was followed by incubation with the primary antibodies or appropriate control antibodies in PBS plus 10% FCS overnight at 4°C. If necessary, tissues were incubated with specific Alexa Fluor–conjugated secondary antibodies in PBS plus 10% FCS for 3 h at 4°C. The samples were imaged at 20°C using a LSM 5 PASCAL laser-scanning confocal microscope (Carl Zeiss) incorporating a 40× water-dipping objective (numerical aperture (NA) 0.75) or a 63× oil-immersion objective (NA 1.4). Z-stack images of postcapillary venules (within a diameter of 20–50 µm) were captured using the multiple track scanning mode at every 1 µm (40×) or 0.4 µm (63×) of tissue depth at a resolution of 1,024 × 1,024 pixels in the x × y plane, corresponding to a voxel size of ∼0.26 × 0.26 × 1/0.4 µm in x × y × z, respectively. Confocal gain, offsets, and laser power were first set on samples stained with isotype control antibodies before being applied for analysis of tissues stained for specific molecules of interest. Resulting confocal images were then analyzed using 3D reconstruction software such as ImageJ (National Institutes of Health) and IMARIS (Bitplane). Postcapillary venules, expressing pericytes and not smooth muscle cells, were identified by vascular morphology, localization within the microcirculation and flow profile. The identification of pericytes in these vessels by this mode was confirmed by immunostaining of tissues for pericyte markers such as PDGFRβ, SMA22α, and NG2. Neutrophil transmigration was quantified using IMARIS, as previously described (Wang et al., 2006; Voisin et al., 2010). To quantify the size of gaps between adjacent pericytes confocal images were 3D reconstructed and split in half in silico along the longitudinal vessel axis using ImageJ. Resulting image sections of semivessels were transformed into grayscale intensity projection and gaps between adjacent pericytes, as detected by αSMA-negative regions, were measured manually. Unstimulated and saline-injected samples were pooled because of identical results. To assess ICAM-1, PDGFRβ, KC, IL-1RI, TNFRI, and TNFRII expression on postcapillary venules, the mean fluorescence intensity (MFI) of tissues stained with control isotype-matched antibodies and tissues stained for specific molecules of interest were determined using IMARIS software. To analyze ECs and pericytes separately, an isosurface was created representing exclusively the endothelium or the pericyte sheath. This parameter depicts the limitation of the volume of interest in which IMARIS determines the MFI of other channels. Isosurfaces embodying the EC or pericyte layer were built by using the channel showing immunofluorescence labeling of PECAM-1 or αSMA as a source, respectively. PECAM-1, ICAM-1, or PDGFRβ labeling was achieved by i.s. injection of 2, 5, or 10 µg anti–PECAM-1–Alexa Fluor 647, anti–ICAM-1–Alexa Fluor 488, or purified anti-PDGFRβ antibodies, respectively, in 400 µl saline. 30 min to 2 h later, mice were sacrificed, the vasculature was washed using 10 ml saline (containing 10% heparin), and cremaster muscles were dissected from the mice for subsequent ex vivo whole-mount immunofluorescence staining. Quantification of expression of molecules of interest was expressed as the MFI for specifically stained tissues minus the MFI of samples stained with an appropriate isotype control antibody.

Analysis of expression levels of ICAM-1 and KC in pericyte gap borders. To quantify the expression levels of ICAM-1 and KC on pericyte cell body and pericyte gap borders, 3D images of cremaster tissues labeled for αSMA, PECAM-1, and ICAM-1 or KC, as described in the previous section, were analyzed by IMARIS and ImageJ software. In brief, an isosurface was produced from the PECAM-1 channel and a new channel-mask of ICAM-1 positive, PECAM-1 negative voxels (i.e., ICAM-1 staining outside PECAM-1 volume) was created from this isosurface. A second isosurface from αSMA channel was then generated and another new channel-mask for ICAM-1 positive, αSMA positive, PECAM-1 negative voxels (i.e., ICAM-1 staining in αSMA volume excluding PECAM-1 volume) from this isosurface was created. 2D projection images were then generated on the αSMA channel and the new ICAM-1–positive, αSMA-positive, PECAM-1–negative channel mask. Images of half vessels were then imported into ImageJ software to measure the area and intensity of ICAM-1 in both gap borders and pericyte sheath. Borders of pericyte gaps were defined as regions within the αSMA channel 2 µm away from the gap border. Area of pericyte gaps was manually measured as described in the previous section.

Confocal IVM. Confocal IVM was used to directly observe changes in pericyte morphology and to study leukocyte/pericyte interactions within cremasteric postcapillary venules upon TNF stimulation in real-time in 3D, using α*SMA-RFPcherry x Lys-EGFP-ki* mice. To elicit leukocyte recruitment and enlargement of gaps between adjacent pericytes, animals were sedated via i.m. injection of 1ml/kg anesthetic (40 mg/kg ketamine and 2 mg/kg xylazine in saline) and were subsequently subjected to i.s. injection of TNF (300 ng/400 µl saline). TNF was co-administered with a nonblocking anti–mouse Alexa Fluor 647–labeled PECAM-1 antibody (clone C390, 2 µg) to visualize the endothelium as previously described (Woodfin et al., 2011). Specificity of this EC junctional staining was confirmed using PECAM$^{-/-}$ mice and an isotype control antibody. 2 h later, mice were prepared for confocal IVM as previously detailed (Woodfin et al., 2011). In brief, mice were anesthetized by i.p. injection of ketamine (100 mg/kg) and xylazine (10 mg/kg) and maintained at 37°C on a custom-built, heated microscope stage. The cremaster muscle was exteriorized, pinned out flat over the optical window of the stage, and superfused with warm Tyrode's solution. During confocal IVM, z-stack images of a postcapillary venule (analyzed vessels were largely within a diameter of 20–50 µm) were captured every minute using a Leica SP5 confocal microscope (Leica) incorporating a 20× water-dipping objective (NA 1.0) for 2 h. Images were acquired with sequential scanning of different channels at a resolution of 1,024 × 512 pixels in the x × y plane and 0.7-µm steps in z-direction, corresponding to a voxel size of ∼0.23 × 0.23 × 0.7 µm in x × y × z, respectively. Throughout the experiment, cremaster muscles were constantly superfused with warm Tyrode's salt solution. For ICAM-1–, Mac-1–, and LFA-1–blocking experiments, blocking antibodies or rat IgG2b (anti–ICAM-1/Mac-1 isotype) or IgG2a (anti–LFA-1 isotype) control antibodies were administered (i.s. 50 µg) 2 h after TNF stimulation and 30 min before exteriorization of the cremaster muscle for confocal IVM. This protocol did not effect the early luminal neutrophil-EC interactions, and thus enabled the analysis of neutrophil responses after TEM. To validate the inhibitory effect of the blocking anti–ICAM-1 mAb, in some experiments the anti–ICAM-1 mAb was co-injected locally with TNF. In these studies, the anti–ICAM-1 mAb significantly inhibited neutrophil adhesion to ECs within the vascular lumen and by extension markedly suppressed neutrophil transmigration. To control for potential Fc binding effects of the anti–ICAM-1 mAb on neutrophil crawling parameters, the effect of a rat anti–mouse PDGFRβ mAb (pericyte binding) was also tested using the same dose and injection protocol. Two nonbinding rat IgG isotype control antibodies (IgG2a and IgG2b) were also tested and, collectively, no differences were detected between untreated and control mAb-treated (including the anti-PDGFRβ mAb) groups. The resulting 4D confocal image sequences were analyzed offline using IMARIS software, which renders the optical sections of half vessels into 3D models, thereby enabling the dynamic interaction of leukocytes and the vessel wall to be observed, tracked, and analyzed. All images and videos show half vessels to enable clear visualization from only one luminal or abluminal side of the vessel wall.

Analysis of neutrophil behaviors. Neutrophil responses in 4D were quantified using the IMARIS software through analysis of 4D confocal image sequences obtained via confocal intravital. Specifically, parameters were established for investigating the profile and dynamics of neutrophil transmigration through the endothelial layer and the pericyte sheath. For each image sequence, only transmigration events were analyzed that were clearly visible in terms of their location and dynamics and were imaged in full in terms of TEM and transmigration through the pericyte sheath. Here, recordings were conducted on half-vessels to enable clear visualization of migratory events through the different components of the venular wall in 3D. On average, 70 migratory events were analyzed from 4–7 mice per group. The duration of TEM was quantified from the first frame showing a disruption of PECAM-1 labeling to the frame in which the neutrophil had fully transmigrated through the endothelium, as previously described (Woodfin et al., 2011). From this frame onwards, abluminal crawling was analyzed to the frame in which the neutrophil had found the gap in the pericyte layer that was used for breaching the pericyte sheath. Duration of transmigration through the pericyte layer was quantified starting from this frame to the frame in which the neutrophil had fully transmigrated through the gap and entered the extravascular tissue. Individual neutrophil migration paths were tracked manually using IMARIS and the generated cell tracks were subsequently used to quantify the following parameters: (a) duration of transmigration (minutes), (b) speed of migration (micrometers/second), (c) track length (micrometers), (d) venular wall track displacement length (i.e., length in micrometers of the shortest connection between the end of TEM to the point when a neutrophil initiates to breach the pericyte layer), and (e) track straightness (ratio of track displacement length to track length). Other parameters of cell morphology, such as leukocyte sphericity, flattening, and elongation, were also quantified using IMARIS software after the generation of an isosurface on neutrophils at different stage of their migration (i.e., cells adherent or crawling luminally along the endothelium, abluminal crawling between ECs and pericytes, and when fully migrated into the extravascular space). This model was also used to quantify the size of pericyte gaps used by transmigrating neutrophils to breach the pericyte layer.

Culture of C3H/10T1/2 cells. The cell line C3H/10T1/2 (clone 8) was purchased from the European Collection of Cell Cultures. These murine fibroblasts isolated from a line of C3H mouse embryo cells (Reznikoff et al., 1973) show pericyte/smooth muscle cell–like properties and express markers of the pericyte/SMC lineage such as αSMA, PDGFRβ, SM22α, and NG2 (as shown by flow cytometry). C3H/10T1/2 cells were cultured at subconfluent density according to the supplier's protocol.

Flow cytometry. C3H/10T1/2 cells were harvested using 0.02% EDTA and were subsequently immunostained for IL-1RI, TNFRI, TNFRII, or an Armenian hamster isotype control antibody. The cells were then incubated with specific anti–hamster secondary antibodies conjugated with biotin. The biotinylated anti–Armenian hamster secondary antibody was detected using streptavidin conjugated with Alexa Fluor 488. Samples were analyzed using a FACSCalibur flow cytometer (BS) and the flow cytometry analysis software FlowJo.

Transfection of C3H/10T1/2 cells with Lifeact-eGFP. To analyze shape change of C3H/10T1/2 cells in response to inflammatory cytokines, fluorescence time-lapse microscopy was performed in cells transfected with the F-actin probe Lifeact-eGFP (Riedl et al., 2008; a gift from M. Sixt, Institute of Science and Technology, Klosterneuburg, Austria) using established protocols (Alexopoulou et al., 2008). In brief, pmeGFP-N1-Lifeact plasmid DNA was transfected using a modified Lipofectamine-based (Invitrogen) protocol. DNA–lipid complexes were generated in serum-free media as described by the manufacturer and used to resuspend a C3H10T1/2 cell pellet containing 3.5 × 10^5 cells that had been previously washed with serum-free DME. After 10 min of incubation at room temperature, the cell suspension was transferred into a well of a 6-well plate containing 2 ml warm normal

growth medium. Fresh medium containing 1 mg/ml Geneticin (Invitrogen) was added after 24 h.

Fluorescence time-lapse microscopy and quantification of cell eccentricity. To perform fluorescence time lapse experiments, Lifeact-eGFP transfected C3H/10T1/2 cells were seeded into 6-well plate dishes at a density of 3.5×10^5 cells/well in normal growth medium 48 h before the experiment. The plates were transferred into the heated chamber of an Olympus IX81 motorized inverted microscope (Olympus Medical) and incubated at 37°C throughout the experiment. Pictures of three different fields of view per dish were taken every 10 min for 4 h using an air long working distance 20× objective (NA 0.45). After the capture of the first image, the inflammatory cytokines IL-1β (1, 10, or 100 ng/ml) or TNF (10 or 100 ng/ml) or vehicle control (PBS) were added to the cells. Time-lapse images were then analyzed using the 3D imaging software IMARIS to track and quantify cell eccentricity (the ratio of cell length to cell width). Cell length was quantified as the longest side of the cell in the direction of cell elongation. Cell width measurement was taken perpendicularly to the middle of the cell length. For all three fields of view cell eccentricity was measured for at least five cells and the mean cell eccentricity was determined for each field of view. The overall mean cell eccentricity was then plotted per dish for each time point, and normalized to the general mean cell eccentricity at time point 0 h (time point captured before the addition of cytokines or vehicle control).

Statistics. Data were plotted and statistically analyzed using Prism (GraphPad Software). Results were expressed as means ± SEM, and significant differences between multiple groups were identified by one-way analysis of variance, followed by Newman-Keuls Multiple Comparison Test. Whenever two groups were compared, Student's *t* test was used. P-values < 0.05 were considered significant.

Online supplemental material. Video 1 shows the development of an inflammatory response as induced by TNF in a cremaster muscle venule of an aSMA-RFPcherry x Lys-EGFP-ki mouse immunostained in vivo for EC junctions with the nonblocking C390 anti–PECAM-1 mAb and as observed by real-time confocal microscopy in vivo. Video 2 and Videos 3–5 are four examples of abluminal crawling of neutrophils along pericyte processes as observed by live confocal microscopy in vivo in a cremasteric venule of an aSMA-RFPcherry x Lys-EGFP-ki mouse after TNF-stimulation. Videos 2 and 3 are from the same image sequence with or without the endothelium being visible, respectively. Video 6 shows a pericyte layer hot spot where multiple neutrophils are migrating through the same gap between adjacent pericytes in a cremasteric postcapillary venule of an *αSMA-RFPcherry x Lys-EGFP-ki* mouse, as observed by live confocal microscopy in vivo. Online supplemental material is available at http://www.jem.org/cgi/content/full/jem.20111622/DC1.

This work was supported by funds from the Wellcome Trust (081172/Z/06/Z) to S. Nourshargh. D. Proebstl was supported by a Medical Research Council PhD studentship awarded to Barts and The London Medical School, and J. Whiteford is an Arthritis Research UK Fellow.

The authors have no conflicting financial interests.

Submitted: 3 August 2011
Accepted: 25 April 2012

REFERENCES

Alexopoulou, A.N., J.R. Couchman, and J.R. Whiteford. 2008. The CMV early enhancer/chicken beta actin (CAG) promoter can be used to drive transgene expression during the differentiation of murine embryonic stem cells into vascular progenitors. *BMC Cell Biol.* 9:2. http://dx.doi.org/10.1186/1471-2121-9-2

Armulik, A., A. Abramsson, and C. Betsholtz. 2005. Endothelial/pericyte interactions. *Circ. Res.* 97:512–523. http://dx.doi.org/10.1161/01.RES.0000182903.16652.d7

Burns, A.R., D.C. Walker, E.S. Brown, L.T. Thurmon, R.A. Bowden, C.R. Keese, S.I. Simon, M.L. Entman, and C.W. Smith. 1997. Neutrophil transendothelial migration is independent of tight junctions and occurs preferentially at tricellular corners. *J. Immunol.* 159:2893–2903.

Christofidou-Solomidou, M., M.T. Nakada, J. Williams, W.A. Muller, and H.M. DeLisser. 1997. Neutrophil platelet endothelial cell adhesion molecule-1 participates in neutrophil recruitment at inflammatory sites and is down-regulated after leukocyte extravasation. *J. Immunol.* 158:4872–4878.

Cohen, M.P., R.N. Frank, and A.A. Khalifa. 1980. Collagen production by cultured retinal capillary pericytes. *Invest. Ophthalmol. Vis. Sci.* 19:90–94.

Edelman, D.A., Y. Jiang, J. Tyburski, R.F. Wilson, and C. Steffes. 2006. Pericytes and their role in microvasculature homeostasis. *J. Surg. Res.* 135:305–311. http://dx.doi.org/10.1016/j.jss.2006.06.010

Faust, N., F. Varas, L.M. Kelly, S. Heck, and T. Graf. 2000. Insertion of enhanced green fluorescent protein into the lysozyme gene creates mice with green fluorescent granulocytes and macrophages. *Blood.* 96:719–726.

Feng, D., J.A. Nagy, K. Pyne, H.F. Dvorak, and A.M. Dvorak. 1998. Neutrophils emigrate from venules by a transendothelial cell pathway in response to FMLP. *J. Exp. Med.* 187:903–915. http://dx.doi.org/10.1084/jem.187.6.903

Hirschi, K.K., and P.A. D'Amore. 1996. Pericytes in the microvasculature. *Cardiovasc. Res.* 32:687–698.

Hobbs, J.A., R. May, K. Tanousis, E. McNeill, M. Mathies, C. Gebhardt, R. Henderson, M.J. Robinson, and N. Hogg. 2003. Myeloid cell function in MRP-14 (S100A9) null mice. *Mol. Cell. Biol.* 23:2564–2576. http://dx.doi.org/10.1128/MCB.23.7.2564-2576.2003

Katori, M., T. Oda, and K. Nagai. 1990. A site of action of dexamethasone on leukocyte extravasation in microcirculation. *Agents Actions.* 29:24–26. http://dx.doi.org/10.1007/BF01964709

Kerkar, S., M. Williams, J.M. Blocksom, R.F. Wilson, J.G. Tyburski, and C.P. Steffes. 2006. TNF-alpha and IL-1beta increase pericyte/endothelial cell co-culture permeability. *J. Surg. Res.* 132:40–45. http://dx.doi.org/10.1016/j.jss.2005.06.033

Kolyada, A.Y., K.N. Riley, and I.M. Herman. 2003. Rho GTPase signaling modulates cell shape and contractile phenotype in an isoactin-specific manner. *Am. J. Physiol. Cell Physiol.* 285:C1116–C1121.

Kutcher, M.E., and I.M. Herman. 2009. The pericyte: cellular regulator of microvascular blood flow. *Microvasc. Res.* 77:235–246. http://dx.doi.org/10.1016/j.mvr.2009.01.007

Kutcher, M.E., A.Y. Kolyada, H.K. Surks, and I.M. Herman. 2007. Pericyte Rho GTPase mediates both pericyte contractile phenotype and capillary endothelial growth state. *Am. J. Pathol.* 171:693–701. http://dx.doi.org/10.2353/ajpath.2007.070102

Ley, K., J.B. Baker, M.I. Cybulsky, M.A. Gimbrone Jr., and F.W. Luscinskas. 1993. Intravenous interleukin-8 inhibits granulocyte emigration from rabbit mesenteric venules without altering L-selectin expression or leukocyte rolling. *J. Immunol.* 151:6347–6357.

Ley, K., C. Laudanna, M.I. Cybulsky, and S. Nourshargh. 2007. Getting to the site of inflammation: the leukocyte adhesion cascade updated. *Nat. Rev. Immunol.* 7:678–689. http://dx.doi.org/10.1038/nri2156

Maier, C.L., and J.S. Pober. 2011. Human placental pericytes poorly stimulate and actively regulate allogeneic CD4 T cell responses. *Arterioscler. Thromb. Vasc. Biol.* 31:183–189. http://dx.doi.org/10.1161/ATVBAHA.110.217117

Mandarino, L.J., N. Sundarraj, J. Finlayson, and H.R. Hassell. 1993. Regulation of fibronectin and laminin synthesis by retinal capillary endothelial cells and pericytes in vitro. *Exp. Eye Res.* 57:609–621. http://dx.doi.org/10.1006/exer.1993.1166

Muller, W.A. 2009. Mechanisms of transendothelial migration of leukocytes. *Circ. Res.* 105:223–230. http://dx.doi.org/10.1161/CIRCRESAHA.109.200717

Murphy, D.D., and R.C. Wagner. 1994. Differential contractile response of cultured microvascular pericytes to vasoactive agents. *Microcirculation.* 1:121–128. http://dx.doi.org/10.3109/10739689409148267

Mydel, P., J.M. Shipley, T.L. Adair-Kirk, D.G. Kelley, T.J. Broekelmann, R.P. Mecham, and R.M. Senior. 2008. Neutrophil elastase cleaves laminin-332 (laminin-5) generating peptides that are chemotactic for neutrophils. *J. Biol. Chem.* 283:9513–9522. http://dx.doi.org/10.1074/jbc.M706239200

Nourshargh, S., P.L. Hordijk, and M. Sixt. 2010. Breaching multiple barriers: leukocyte motility through venular walls and the interstitium. *Nat. Rev. Mol. Cell Biol.* 11:366–378. http://dx.doi.org/10.1038/nrm2889

Pham, C.T. 2006. Neutrophil serine proteases: specific regulators of inflammation. *Nat. Rev. Immunol.* 6:541–550. http://dx.doi.org/10.1038/nri1841

Phillipson, M., B. Heit, P. Colarusso, L. Liu, C.M. Ballantyne, and P. Kubes. 2006. Intraluminal crawling of neutrophils to emigration sites: a molecularly distinct process from adhesion in the recruitment cascade. *J. Exp. Med.* 203:2569–2575. http://dx.doi.org/10.1084/jem.20060925

Puls, A., A.G. Eliopoulos, C.D. Nobes, T. Bridges, L.S. Young, and A. Hall. 1999. Activation of the small GTPase Cdc42 by the inflammatory cytokines TNF(alpha) and IL-1, and by the Epstein-Barr virus transforming protein LMP1. *J. Cell Sci.* 112:2983–2992.

Reznikoff, C.A., D.W. Brankow, and C. Heidelberger. 1973. Establishment and characterization of a cloned line of C3H mouse embryo cells sensitive to postconfluence inhibition of division. *Cancer Res.* 33:3231–3238.

Riedl, J., A.H. Crevenna, K. Kessenbrock, J.H. Yu, D. Neukirchen, M. Bista, F. Bradke, D. Jenne, T.A. Holak, Z. Werb, et al. 2008. Lifeact: a versatile marker to visualize F-actin. *Nat. Methods.* 5:605–607. http://dx.doi.org/10.1038/nmeth.1220

Rowe, R.G., and S.J. Weiss. 2008. Breaching the basement membrane: who, when and how? *Trends Cell Biol.* 18:560–574. http://dx.doi.org/10.1016/j.tcb.2008.08.007

Schlaeger, T.M., Y. Qin, Y. Fujiwara, J. Magram, and T.N. Sato. 1995. Vascular endothelial cell lineage-specific promoter in transgenic mice. *Development.* 121:1089–1098.

Shaner, N.C., R.E. Campbell, P.A. Steinbach, B.N. Giepmans, A.E. Palmer, and R.Y. Tsien. 2004. Improved monomeric red, orange and yellow fluorescent proteins derived from Discosoma sp. red fluorescent protein. *Nat. Biotechnol.* 22:1567–1572. http://dx.doi.org/10.1038/nbt1037

Shepro, D., and N.M. Morel. 1993. Pericyte physiology. *FASEB J.* 7:1031–1038.

Sims, D.E. 2000. Diversity within pericytes. *Clin. Exp. Pharmacol. Physiol.* 27:842–846. http://dx.doi.org/10.1046/j.1440-1681.2000.03343.x

Sixt, M., R. Hallmann, O. Wendler, K. Scharffetter-Kochanek, and L.M. Sorokin. 2001. Cell adhesion and migration properties of beta 2-integrin negative polymorphonuclear granulocytes on defined extracellular matrix molecules. Relevance for leukocyte extravasation. *J. Biol. Chem.* 276:18878–18887. http://dx.doi.org/10.1074/jbc.M010898200

Speyer, C.L., C.P. Steffes, and J.L. Ram. 1999. Effects of vasoactive mediators on the rat lung pericyte: quantitative analysis of contraction on collagen lattice matrices. *Microvasc. Res.* 57:134–143. http://dx.doi.org/10.1006/mvre.1998.2134

Steadman, R., M.H. Irwin, P.L. St John, W.D. Blackburn, L.W. Heck, and D.R. Abrahamson. 1993. Laminin cleavage by activated human neutrophils yields proteolytic fragments with selective migratory properties. *J. Leukoc. Biol.* 53:354–365.

Sumagin, R., and I.H. Sarelius. 2010. Intercellular adhesion molecule-1 enrichment near tricellular endothelial junctions is preferentially associated with leukocyte transmigration and signals for reorganization of these junctions to accommodate leukocyte passage. *J. Immunol.* 184:5242–5252. http://dx.doi.org/10.4049/jimmunol.0903319

Verbeek, M.M., J.R. Westphal, D.J. Ruiter, and R.M. de Waal. 1995. T lymphocyte adhesion to human brain pericytes is mediated via very late antigen-4/vascular cell adhesion molecule-1 interactions. *J. Immunol.* 154:5876–5884.

Voisin, M.B., A. Woodfin, and S. Nourshargh. 2009. Monocytes and neutrophils exhibit both distinct and common mechanisms in penetrating the vascular basement membrane in vivo. *Arterioscler. Thromb. Vasc. Biol.* 29:1193–1199. http://dx.doi.org/10.1161/ATVBAHA.109.187450

Voisin, M.B., D. Pröbstl, and S. Nourshargh. 2010.Venular basement membranes ubiquitously express matrix protein low-expression regions: characterization in multiple tissues and remodeling during inflammation. *Am. J. Pathol.* 176:482–495. http://dx.doi.org/10.2353/ajpath.2010.090510

Wang, J., M. Juhaszova, L.J. Rubin, and X.J. Yuan. 1997. Hypoxia inhibits gene expression of voltage-gated K+ channel alpha subunits in pulmonary artery smooth muscle cells. *J. Clin. Invest.* 100:2347–2353. http://dx.doi.org/10.1172/JCI119774

Wang, S., J.P. Dangerfield, R.E. Young, and S. Nourshargh. 2005. PECAM-1, alpha6 integrins and neutrophil elastase cooperate in mediating neutrophil transmigration. *J. Cell Sci.* 118:2067–2076. http://dx.doi.org/10.1242/jcs.02340

Wang, S., M.B. Voisin, K.Y. Larbi, J. Dangerfield, C. Scheiermann, M. Tran, P.H. Maxwell, L. Sorokin, and S. Nourshargh. 2006. Venular basement membranes contain specific matrix protein low expression regions that act as exit points for emigrating neutrophils. *J. Exp. Med.* 203:1519–1532. http://dx.doi.org/10.1084/jem.20051210

Woodfin, A., M.B. Voisin, M. Beyrau, B. Colom, D. Caille, F.M. Diapouli, G.B. Nash, T. Chavakis, S.M. Albelda, G.E. Rainger, et al. 2011. The junctional adhesion molecule JAM-C regulates polarized transendothelial migration of neutrophils in vivo. *Nat. Immunol.* 12:761–769. http://dx.doi.org/10.1038/ni.2062

Yadav, R., K.Y. Larbi, R.E. Young, and S. Nourshargh. 2003. Migration of leukocytes through the vessel wall and beyond. *Thromb. Haemost.* 90:598–606.

Yokota, T., Y. Kawakami, Y. Nagai, J.X. Ma, J.Y. Tsai, P.W. Kincade, and S. Sato. 2006. Bone marrow lacks a transplantable progenitor for smooth muscle type alpha-actin-expressing cells. *Stem Cells.* 24:13–22. http://dx.doi.org/10.1634/stemcells.2004-0346